IJC
International Journal of Cancer

Epigenetic determinants of ovarian clear cell carcinoma biology

Ken Yamaguchi[1,2], Zhiqing Huang[1], Noriomi Matsumura[2], Masaki Mandai[3], Takako Okamoto[1], Tsukasa Baba[2], Ikuo Konishi[2], Andrew Berchuck[1] and Susan K. Murphy[1]

[1] Department of Obstetrics and Gynecology, Duke University Medical Center, Durham, NC
[2] Department of Gynecology and Obstetrics, Graduate School of Medicine, Kyoto University, Kyoto, Japan
[3] Department of Obstetrics and Gynecology, Kinki University Faculty of Medicine, Osaka, Japan

Targeted approaches have revealed frequent epigenetic alterations in ovarian cancer, but the scope and relation of these changes to histologic subtype of disease is unclear. Genome-wide methylation and expression data for 14 clear cell carcinoma (CCC), 32 non-CCC and four corresponding normal cell lines were generated to determine how methylation profiles differ between cells of different histological derivations of ovarian cancer. Consensus clustering showed that CCC is epigenetically distinct. Inverse relationships between expression and methylation in CCC were identified, suggesting functional regulation by methylation, and included 22 hypomethylated (UM) genes and 276 hypermethylated (HM) genes. Categorical and pathway analyses indicated that the CCC-specific UM genes were involved in response to stress and many contain hepatocyte nuclear factor (HNF) 1-binding sites, while the CCC-specific HM genes included members of the estrogen receptor alpha (ERalpha) network and genes involved in tumor development. We independently validated the methylation status of 17 of these pathway-specific genes, and confirmed increased expression of HNF1 network genes and repression of ERalpha pathway genes in CCC cell lines and primary cancer tissues relative to non-CCC specimens. Treatment of three CCC cell lines with the demethylating agent Decitabine significantly induced expression for all five genes analyzed. Coordinate changes in pathway expression were confirmed using two primary ovarian cancer datasets ($p < 0.0001$ for both). Our results suggest that methylation regulates specific pathways and biological functions in CCC, with hypomethylation influencing the characteristic biology of the disease while hypermethylation contributes to the carcinogenic process.

Cancer Genetics

Ovarian cancer is the fifth most common cause of cancer death in women[1] and has the worst mortality rate of all gynecologic cancers.[2] Epithelial ovarian cancers are a heterogeneous disease with distinct clinicopathological and molecular features[3] and are classified pathologically into four major histologic subtypes based entirely on tumor cell morphologic criteria: serous adenocarcinoma (SAC), mucinous adenocarcinoma (MAC), endometrioid adenocarcinoma (EAC) and clear cell carcinoma (CCC). Because these histologic subtypes of ovarian cancer have unique clinical characteristics and behavior, histology-specific biomarkers and individualized therapeutic strategies are needed that improve therapeutic options and outcomes. Ovarian CCC is distinct from the other major histologic types of epithelial ovarian cancer[4,5] and often arises from endometriosis. The clinical outcome of advanced-stage CCC is generally poor and this may be related to the relative resistance to conventional platinum- or taxane-based chemotherapies.[6–8] Although the different histologic subtypes of ovarian cancer have been associated with genetic defects, such as *TP53* mutations in high-grade SAC, *PTEN* and *CTNNBI* mutations in EAC and *KRAS* mutations in MAC, the molecular features of CCC have remained elusive.[9] Recent genome-wide technologies have revealed frequent *ARID1A* mutations[10,11] and overexpression of *HNF1B*[12] in ovarian CCC. We previously identified an ovarian CCC-specific gene signature characterized by activation of the *HNF1B* pathway. Furthermore, some of these signature genes are regulated by DNA methylation.[13]

DNA methylation is an epigenetic mechanism of gene regulation that plays a crucial role in many biological processes including X-chromosome inactivation, genomic imprinting, aging and cancer.[14] In cancer cells, global DNA hypomethylation and aberrant hypermethylation of tumor suppressor genes are well-established mechanisms that contribute to cancer cell transformation.[15] Analysis of individual genes has led to a large number now reported as targets of DNA methylation in ovarian cancer.[1,16] However, genome-wide methylation profiles may be more instructive because the

Key words: ovarian clear cell carcinoma, HNF1, ERalpha, methylation, epigenetic characterization
Additional Supporting Information may be found in the online version of this article
Conflict of interest: Nothing to report
Grant sponsors: American Cancer Society and the Gail Parkins Ovarian Cancer Research Fund
DOI: 10.1002/ijc.28701
History: Received 22 Jan 2013; Accepted 4 Dec 2013; Online 31 Dec 2013
Correspondence to: Susan K. Murphy, Department of Obstetrics and Gynecology, Duke University Medical Center, B226 Levine Science Research Center/Research Drive, Box 91012, Durham, NC 27708, USA, Tel.: +1-919-681-3423, Fax: +1-919-684-5336, E-mail: susan.murphy@duke.edu

What's new?

Ovarian cancer has several subtypes, and although different genetic mutations have been associated with particular subtypes, the molecular characteristics of ovarian clear cell carcinoma remain hazy. Aberrant DNA methylation can turn cells cancerous, and this study compared patterns of gene methylation in ovarian clear cell carcinomas, other ovarian cancer cells, and normal cells. They found that the clear cell carcinomas could indeed be identified by their distinctive pattern of DNA methylation. They found that this methylation pattern increased expression of certain stress response genes, while other genes, with tumor suppressive functions, were stifled.

methylation status of any particular single gene has not been shown to be predictive, diagnostic or prognostic for this disease.[15,17] Higher resolution elucidation of DNA methylation profiles may lead to the discovery of biomarkers for diagnosis, improved methods of classification and disease monitoring as well as to a better understanding of cancer biology. Although several comprehensive DNA methylation analyses have been reported in ovarian cancer, limitations have included a relatively small number of samples, lack of focus on histological subtypes and in the limited number and selection of genes analyzed.[14,17–20] Only four genes (*14-3-3 sigma* as *SFN, PYCARD, WT1* and *HNF1B*) have been reported as aberrantly methylated in CCC.[1,13,16,21] Therefore, epigenetic features that more fully characterize histological subtypes including CCC have yet to be identified.

In this study, our initial objective was to determine if epigenomic patterns could distinguish the various histologic subtypes of ovarian cancer, including CCC. We identified an ovarian CCC methylation profile that was distinct from the other histologic subtypes of ovarian cancer. Through analysis of genes showing strong associations between DNA methylation and levels of transcription, we identified important biological mechanisms contributing to characteristic features of ovarian CCC[4] that appear to be deregulated through coordinate epigenetic modifications in this disease.

Material and Methods

Detailed methods are provided in Supporting Information.

Cell lines and clinical samples

The immortalized noncancerous cell lines were maintained as described.[22–24] Ovarian cancer cell lines, including 14 CCC and 32 non-CCC cell lines (Supporting Information Table 1), were cultured in RPMI1640/FBS/pen-strep medium (Sigma-Aldrich, St. Louis, MO) with 10% heat-inactivated fetal bovine serum (v/v; Invitrogen, Carlsbad, CA) in an atmosphere of 5% CO_2 at 37°C. The short tandem repeat (STR) genotypes of all ovarian cancer cell lines were analyzed to authenticate the cell lines using either the PowerPlex® 1.2 System (Promega, Madison, WI) at The Fragment Analysis Facility of Johns Hopkins University or the AmpFℓSTR® Identifiler® Plus PCR Amplification Kit (Applied Biosystems, Carlsbad, CA) at the University of Colorado Cancer Center, DNA Sequencing and Analysis Core. The STR genotypes of ovarian cancer cell lines that are available from ATCC, RIKEN BioResource Center Cell Bank or the Japanese Collection of Research Bioresources (JCRB) Cell Bank were identical to the source genotypes as reported within their respective STR databases and all other noncommercially available cell lines were shown to be derived from females with unique genotypes.

Tissue specimens were derived from 85 patients with ovarian cancer treated at Duke University Medical Center, (13 CCC, 53 SAC, 11 EAC and eight MAC) and from eight patients without malignant disease (four ovarian surface epithelium samples and four fallopian tube epithelium samples). All patients provided written informed consent and specimens were used under a protocol approved by the Duke University Institutional Review Board. For all tumor specimens, representative sections were mounted on slides and stained with hematoxylin and eosin to confirm that at least 60% of the cellular content comprised cancer cells with less than 20% necrosis. Tumors were histologically classified according to World Health Organization (WHO) criteria.

Extraction of genomic DNA and bisulfite treatment

Genomic DNA was extracted from cells cultured in 10-cm dishes to 70–90% confluence using the QIAamp® DNA Mini Kit (Qiagen, Valencia, CA) or from 5 to 20 mg of clinical tissues using the AllPrep® DNA/RNA/Protein Mini Kit (Qiagen) for methylation beadchip analysis. Puregene Reagents (Qiagen) were used for DNA extraction after Decitabine treatment (see below). Five hundred nanograms of genomic DNA was bisulfite modified using the EZ DNA Methylation™ Kit (Zymo Research, Irvine, CA) according to the manufacturer's protocol for the Infinium methylation assay, and 800 ng of genomic DNA was bisulfite modified using the same kit but according to standard protocol for methylation analysis of individual genes.

Illumina Infinium HumanMethylation BeadChip Assays

Bisulfite-converted genomic DNA was analyzed using the Illumina Infinium HumanMethylation27 BeadChip for cell line samples (GEO Accession Number GSE51688) and HumanMethylation450 Beadchip for clinical tissue specimens (GEO Accession Number GSE51820) (Illumina, San Diego, CA). The HumanMethylation450 BeadChip includes 90% of the content contained on the HumanMethylation27 BeadChip (http:// dl.dropbox.com/u/6904769/50CellLines_b-value_submission.txt.zip). Chip processing was performed according

to the manufacturer's protocol by Expression Analysis (Durham, NC), an Illumina Certified Service Provider. Data were extracted using Illumina GenomeStudio v2010.3 software (Illumina). Methylation values for each CpG locus are represented as β-values, a quantitative measure of DNA methylation, with levels ranging from 0 (completely unmethylated) to 1 (completely methylated). Bisulfite conversion efficiency (*i.e.*, the conversion of non-CpG cytosines to uracils) was assessed for all samples by Pyrosequencing (see below) before data generation using the Illumina BeadChips.

Methylation-specific polymerase chain reaction

DNA methylation of estrogen receptor alpha (ERalpha) network genes (*ESR1, BMP4, DKK1, SOX11, SNCG* and *MOSC1*) was validated using methylation-specific polymerase chain reaction (MS-PCR). Primer sequences and PCR conditions are provided in Supporting Information Table 2a.

Pyrosequencing

All primers for pyrosequencing assays were designed using PSQ assay design software version 1.0.6 (Biotage, Uppsala, Sweden). The pyrosequencing assays were designed such that we analyzed the same CpG sites as those present on the Illumina BeadChip for 11 genes (*ESR1, HNF1A, HNF1B, C14orf105, KIF12, MIA2, PAX8, SERPINA6, SGK2, SRC* and *TM4SF4*) and for adjacent CpG sites for the *F2* gene. Primer sequences and PCR conditions are shown in Supporting Information Table 2b. Methylation values for each CpG site were calculated using Pyro Q-CpG software 1.0.9 (Biotage).

Real-time reverse transcription-polymerase chain reaction

Two micrograms of total RNA prepared from 36 ovarian cancer cell lines (13 CCC and 23 non-CCC; using RNA Stat60, Teltest, Friendswood, TX) or 49 frozen tissues (13 CCC and 36 non-CCC; using the AllPrep® DNA/RNA/Protein Mini Kit; Qiagen) were used to generate cDNA in a 40 µl volume with the Superscript II kit (Invitrogen). Two microliters of the cDNA was used as template for PCR using TaqMan assays in a 20 µl volume (Applied Biosystems) for *HNF1B* (Hs01001602), *SGK2* (Hs00367639), *C14orf105* (Hs00216847), *F2* (Hs01011988), *ESR1* (Hs00174860), *CRIP1* (Hs00832816), *SOX11* (Hs00846583), *IGFBP4* (Hs01057900) and *BMP4* (Hs00370078). *B2M* (Hs 00187842) was used as an internal control. Relative expression was calculated using the delta delta Ct method.

5-Aza-2′-deoxycytidine (Decitabine) treatment

RMG-2, RMG-5 and KOC-7C cell lines were seeded into six-well plates and the following day they were treated in triplicate by adding RPMI1640/FBS/pen-strep media (mock) or the same media containing 5 µM 5-aza-2′-deoxycytidine (Decitabine; Sigma-Aldrich). Media was replaced daily (with/without Decitabine as relevant) for 3 days after which the cells had reached 70–90% confluence and were harvested for DNA extraction as described above or RNA extraction using RNA Stat60 (Teltest). Real-time reverse transcription (RT)-PCR and pyrosequencing analyses were performed as described above.

Bioinformatics

Identification of genes showing differential methylation. Identification of genes differentially methylated between groups was done by comparing β-values using unpaired *t*-tests with thresholds of $p < 0.01$ and difference of average β-values >0.2 (20% methylation) for the comparison between ovarian cancer cell lines and normal cells or between CCC and non-CCC. Genes annotated by gene name or gene ID (Illumina annotation file) were used for the analyses.

Unsupervised consensus clustering. ConsensusCluster software[25] was used to evaluate the similarity between genes or specimens.

Identification of genes regulated by DNA methylation in ovarian cancer. Two cell line microarray datasets [Gene Expression Omnibus (GEO) Accession Number: GSE25428 and GSE29175[13,26] were used for the identification of candidate genes whose mRNA expression levels are regulated by DNA methylation in ovarian cancer. The ComBat normalizing algorithm was used before performing any analysis to reduce the likelihood of batch effects.[27] Candidate genes functionally regulated by methylation were identified based on the following criteria: (*i*) the *p*-value of unpaired Student *t*-tests is less than 0.01; (*ii*) the average β-value difference is more than 0.2 (20% methylation) between 14 CCC cell lines and 32 non-CCC cell lines and (*iii*) a significant inverse correlation ($p < 0.05$) between expression microarray values and β-values from the Infinium assay for the 42 ovarian cancer cell lines with gene expression data.

Categorical analyses. The biological characteristics of the CCC-specific methylation signature were evaluated using the enrichment of Molecular Signatures Database (MSigDB) gene sets (v2.5 updated April 7 2008)[28] with the R package allez 1.0.[29] Briefly, for each gene set, the proportion of the annotated genes in the CCC hypermethylated or hypomethylated gene sets was compared to that for all probeset genes. A gene set was considered significantly enriched if the *z*-score was more than 4.0.[30]

Pathway analyses. The relationship of hypermethylated or hypomethylated genes to particular pathways was evaluated using MetaCore™ software (GeneGo; http://www.genego.com/), an integrated knowledge database and software suite for evaluation of the association between a particular gene list and known pathways.

Heatmap of β-values and expression. Absolute β-values are represented by color gradient intensity, from white; β-value =0, to red; β-value =1, using Java TreeView (http://jtreeview.sourceforge.net/). Average-linkage hierarchical clustering was performed in published expression microarray datasets representing clinical ovarian cancer samples (GSE6008 and

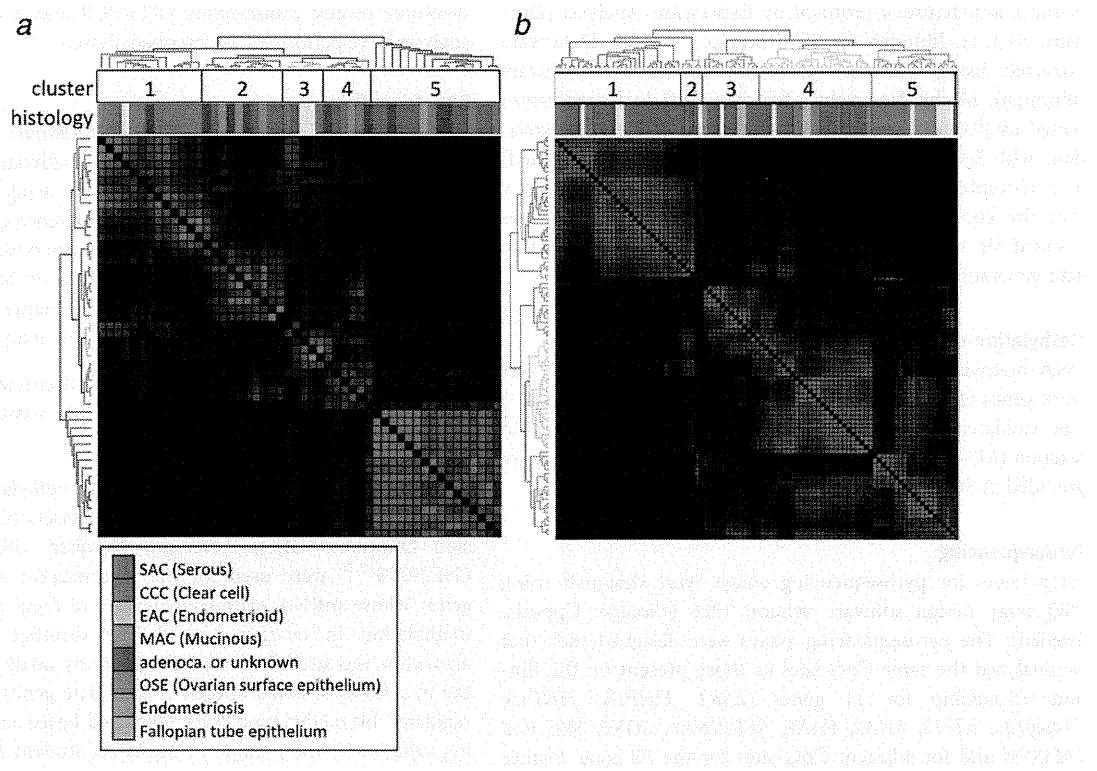

Figure 1. Consensus clustering of DNA methylation profiles for 46 ovarian cancer and four noncancerous cell lines (*a*), and 85 clinical ovarian cancer specimens and eight normal counterparts (*b*). Red–black coloration represents the similarity of methylation profiles between samples from similar to divergent methylation patterns, respectively. The same specimens are ordered identically in the individual rows and columns. The colored dendrogram indicates the five different clusters and the color bar indicates the histological subtype derivation of each specimen.

GSE2109[31,32]) using genes transcriptionally regulated by DNA methylation with Cluster version 3.0 (http://rana.lbl.gov/eisen/).

Statistical analyses

The Student's *t*-test was used to compare continuous variables between groups. Fisher's exact test was used for analysis of categorical variables. Correlations between expression microarray values and methylation β-values from the Infinium assay or between β-values and % methylation values from pyrosequencing were evaluated using Pearson's correlation. *p*-values less than 0.05 were considered statistically significant.

Results

Divergent methylation profiles between ovarian cancer cells and noncancerous cells

By comparing methylation β-values, 2,003 genes (2,561 CpG sites) of a total possible 14,495 genes (27,578 CpG sites) (13.8%) in ovarian cancer cell lines showed methylation levels that differed relative to noncancerous specimens (Supporting Information Table 3). Of these differentially methylated genes, 1,870 genes (2,404 CpG sites; 93.4%) were hypermethylated (HM), whereas only 139 genes (157 CpG sites; 7.0%) were hypomethylated (UM) in ovarian cancer cell lines.

In the clinical samples analyzed with the larger probeset, 3,432 genes (6,919 CpG sites) of 21,231 genes (365,860 CpG sites) (16.2%) showed methylation levels that differed compared to normal specimens. Of the differentially methylated genes, 2,383 genes (4,830 CpG sites; 65.6%) were HM, whereas 1,253 genes (2,089 CpG sites; 34.5%) were UM in ovarian cancer tissues (Supporting Information Table 3).

CCCs possess a unique methylation profile

Unsupervised consensus clustering generated a distinct CCC-specific cluster in the cell line dataset (Fig. 1*a*). The noncancerous cell lines clustered together with nine of 16 SAC (56.3%) cell lines. This data indicates that CCCs possess a distinct epigenomic pattern when compared to the other histologic types of ovarian cancer and noncancerous specimens. Similar to the clustering results in the cell lines, a distinctive CCC-specific cluster was again generated from analysis of clinical specimens. Like the cell lines, 25 of 51 (49.0%) SAC clinical specimens clustered together with normal specimens (Fig. 1*b*). Among the tissue specimens, six of eight MAC and five of 11 EAC samples were grouped within the cluster

containing the majority of the CCC samples. However, both the MAC and EAC subclusters are distinct from the CCC subcluster, indicating that the methylation profiles of MAC and EAC share higher similarity to CCC when compared to the other tissue specimens.

To evaluate the similarity between cell lines and clinical samples, the number of differentially methylated probes that overlap between these datasets was determined among the 25,978 CpG probes in common between the HumanMethylation27 and HumanMethylation450 BeadChips. Of these evaluable CpG probes, 1,042 and 77 CpGs showed hypermethylation in CCC compared to non-CCC cell lines and patient specimens, respectively, with a statistically significant overlap of 25 probes ($p < 0.0001$). We also found that the cell lines and clinical samples had 54 and 53 CpG probes showing hypomethylation, respectively, in CCC relative to non-CCC, with six CpG probes in common, a finding that is also statistically significant ($p < 0.0001$). These 25 hypermethylated and six hypomethylated probes are shown in Supporting Information Tables 4a and 4b. These results support that there are specific methylation profiles in cell lines that are also detectable in patient samples.

Identification of genes transcriptionally regulated by DNA methylation in CCC

Next, we examined the biological significance of the CCC-specific DNA methylation. For this purpose, the genes most likely to be transcriptionally regulated by DNA methylation in CCC were identified using cell line data because of the availability of both methylation and expression microarray data and the similarity of methylation status between the cell lines and clinical specimens. First, 856 genes (1,042 CpG sites) showed increased methylation, and 44 genes (54 CpG sites) showed decreased methylation in CCC when compared to non-CCC (Supporting Information Fig. 1a). Next, potential functional relationships between expression and methylation of the 856 HM and 44 UM CCC genes were assessed by determining if there were correlations between these values. Of 625 evaluable HM genes, 276 genes showed a significant inverse correlation ($r < -0.3051$, $p < 0.05$) between methylation and expression. Of the 33 evaluable UM genes, 22 showed a significant inverse correlation ($r < -0.3217$, $p < 0.05$) between methylation and expression (Supporting Information Fig. 1b). We considered these 276 HM and 22 UM genes as candidate CCC-specific epigenetically regulated genes (Supporting Information Tables 5a and 5b, respectively).

Hypomethylation of the HNF1 pathway and hypermethylation of estrogen receptor pathway genes in CCC

Biological functions of the 22 CCC-specific UM genes were characterized by analyzing the targeted pathways and "biological process" Gene Ontology (GO) terms. Pathway analysis using MetaCore™ indicated that nine of these 22 UM genes (41%) are members of the HNF1 pathway (Fig. 2*a*). Furthermore, the nine CCC-specific UM HNF1 pathway genes are not randomly deregulated but rather synchronously altered by methylation in CCC (Fig. 2*c*), suggesting that hypomethylation in CCC targets HNF1 pathway genes. Analyses using allez showed significant enrichment of all HNF1-binding motifs among the CCC UM genes including categorical terms V$HNF1_01, RGTTAMWNATT_V$HNF1_01, V$HNF1_Q6 and V$HNF1_C ($p < 0.00001$; Supporting Information Table 6). Allez showed that the 22 CCC UM genes were enriched for stress response-related GO terms including "response to oxidative stress" (z-score > 4.0; Table 1, top).

Among the 276 CCC-specific HM genes, pathway analysis showed that 64 genes were involved in the estrogen receptor pathway (Fig. 2*b*). Similar to the synchronous decreased methylation of HNF1 pathway genes in CCC, these 64 genes exhibit coordinate hypermethylation in CCC relative to non-CCC (Fig. 2*d*). These results indicate that the estrogen receptor pathway is a target of hypermethylation in CCC. A categorical analysis using allez to identify GO terms associated with the HM genes showed that the 276 genes HM in CCC included many with tumor-suppressive functions having GO annotations of "cell cycle arrest" and "negative regulation of cell cycle," and development- and organogenesis-related genes with annotations of "negative regulation of cytoskeleton organization and biogenesis" (Table 1, bottom).

Validation of hypomethylation and increased expression of HNF1 pathway genes in CCC

Eleven hypomethylated genes in the HNF1 pathway (*HNF1A, HNF1B, C14orf105, KIF12, MIA2, PAX8, SERPINA6, SGK2, SRC, TM4SF4* and *F2*) identified through analysis of CCC *versus* noncancerous specimens and from comparisons between CCC *versus* non-CCC cell lines were analyzed by bisulfite pyrosequencing. The ten genes for which the same CpG sites were analyzed showed very strong positive correlations between the Infinium assay β-values and the percent methylation as measured by pyrosequencing ($r > 0.9605$, $p < 0.000001$ for all genes; Supporting Information Fig. 2). Adjacent CpG sites for these same ten genes also showed significant positive correlations between the β-values of the Infinium assay CpG sites and the percent methylation by pyrosequencing, as did the adjacent CpG sites measured for the F2 gene ($0.7494 < r < 0.9906$, $p < 0.000001$ for all genes; Supporting Information Fig. 3). Confirming the results of the methylation beadchip analyses, the pyrosequencing results also showed significantly lower methylation levels in CCC relative to those in non-CCC cell lines for these 11 genes ($p < 0.01$ for all genes; Fig. 3*a*). In 85 clinical ovarian cancer specimens, ten of the 11 HNF1 network genes showed overall hypomethylation in ovarian CCC specimens and six of these 11 genes showed significantly decreased methylation in CCC compared to non-CCC (*HNF1A*, $p = 0.0036$; *HNF1B*, $p = 0.0041$; *C14orf105*, $p = 0.0194$; *SERPINA6*, $p = 0.0291$; *SRC*,

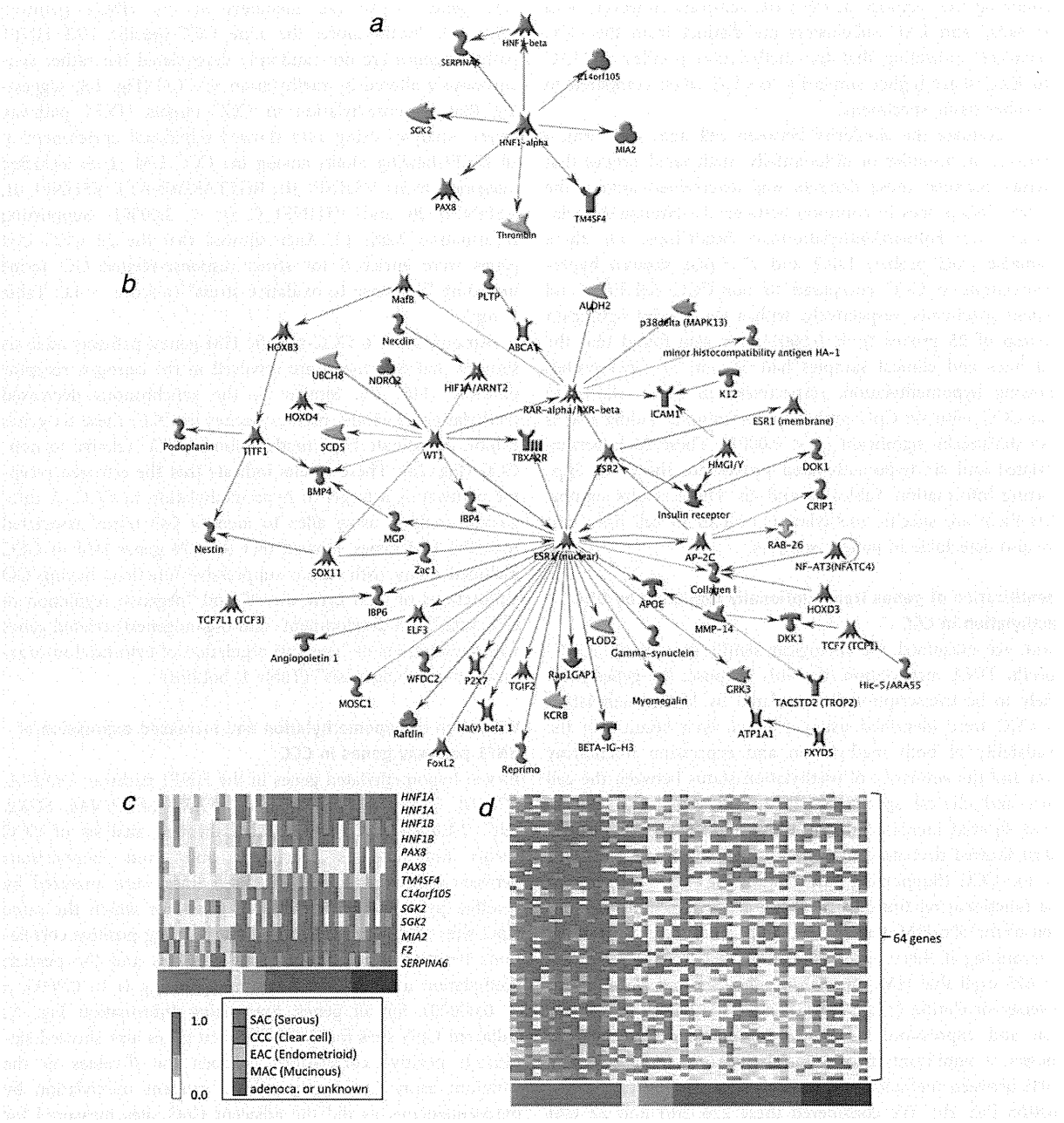

Figure 2. MetaCore™ pathway analyses of the 22 CCC-specific UM genes (*a*) and the 276 CCC-specific HM genes (*b*), and heatmaps showing methylation profiles of nine HNF1 pathway genes (*c*) and 64 ERalpha network genes (*d*) in 46 ovarian cancer cell lines. Of the 22 CCC-specific UM genes for which expression and methylation are inversely correlated, nine were identified as members of the HNF1 transcriptional network (*a*). Of 276 CCC-specific HM genes for which expression and methylation are inversely correlated, 65 were members of the ERalpha (encoded by *ESR1*) network (*b*). In the heatmaps, red to white coloration represents the Infinium β-value from completely methylated to completely unmethylated, respectively. Genes within the HNF1 pathway (*c*) and ERalpha network (*d*) show synchronous hypomethylation and hypermethylation, respectively, in CCC *versus* non-CCC cell lines.

p = 0.0004 and *F2*, p = 0.0003; Fig. 3*b*). When CCC was compared with SAC, eight genes were significantly hypomethylated in CCC (*HNF1A*, p = 0.0007; *HNF1B*, p = 0.0002; *C14orf105*, p = 0.0073; *MIA2*, p = 0.0480; *SERPINA6*, p = 0.0071; *SRC*, $p < 0.0001$; *TM4SF4*, p = 0.0452 and *F2*, $p < 0.0001$; Fig. 3*b* and data not shown).

Table 1. Categorical analysis of "biological process" gene ontology (GO) terms for the 22 UM genes (top) and 276 HM genes (bottom) in CCC

MSigID.c5.bp	*n*-Probes	*z*-Score	*p*-Value
22 CCC-specific UM genes			
POSITIVE REGULATION OF TRANSCRIPTION DNA DEPENDENT[1]	202	8.78	<0.000001
POSITIVE REGULATION OF RNA METABOLIC PROCESS[2]	205	8.70	<0.000001
POSITIVE REGULATION OF TRANSCRIPTION[1]	242	7.90	<0.000001
POSITIVE REGULATION OF NUCLEOBASE NUCLEOSIDE NUCLEOTIDE AND NUCLEIC ACID METABOLIC PROCESS[2]	260	7.58	<0.000001
POSITIVE REGULATION OF CELLULAR METABOLIC PROCESS[2]	396	5.83	<0.000001
POSITIVE REGULATION OF METABOLIC PROCESS[2]	407	5.73	<0.000001
PROTEIN IMPORT INTO NUCLEUS TRANSLOCATION[1]	21	4.66	0.000002
RESPONSE TO OXIDATIVE STRESS[2]	78	4.65	0.000002
TYROSINE PHOSPHORYLATION OF STAT PROTEIN	26	4.14	0.000017
GLUTAMINE FAMILY AMINO ACID METABOLIC PROCESS	27	4.06	0.000025
276 CCC-specific HM genes			
NEGATIVE REGULATION OF CYTOSKELETON ORGANIZATION AND BIOGENESIS[3]	18	7.19	<0.000001
MICROTUBULE POLYMERIZATION OR DEPOLYMERIZATION[3]	21	6.58	<0.000001
PYRIMIDINE NUCLEOTIDE METABOLIC PROCESS	15	5.86	<0.000001
CELL CYCLE ARREST GO 0007050[4]	115	4.78	0.000001
SENSORY ORGAN DEVELOPMENT[3]	23	4.53	0.000003
AEROBIC RESPIRATION	24	4.40	0.000005
NEGATIVE REGULATION OF CELL CYCLE[4]	157	4.33	0.000008
NEGATIVE REGULATION OF CELLULAR COMPONENT ORGANIZATION AND BIOGENESIS[3]	45	4.05	0.000026

[1]GO terms related to transcriptional activation.
[2]GO terms related to stress response.
[3]GO terms related to development and organogenesis.
[4]GO terms related to tumor suppression.

We selected four HNF1B network genes for expression validation studies using both cell lines and clinical specimens. Messenger RNA levels of *HNF1B, F2, C14orf105* and *SGK2* were significantly increased in 13 CCC cell lines compared to 23 non-CCC cell lines ($p = 0.0018$, $p = 0.0057$, $p = 0.0046$ and $p = 0.0158$, respectively; Fig. 4*a*). Clinical samples also showed higher expression for all four genes comparing CCC ($N = 13$) to non-CCC ($N = 36$) specimens (*HNF1B*, $p = 0.0002$; *F2*, $p < 0.0001$; *C14orf105*, $p = 0.0002$ and *SGK2*, $p = 0.0019$; Fig. 4*b*).

We used publicly available ovarian cancer expression microarray datasets representing clinical ovarian cancer samples (GSE6008 and GSE2109) to assess the expression levels of the genes we had identified as functionally regulated by methylation. Supervised hierarchical clustering was performed using only the genes regulated by DNA methylation listed in Supporting Information Tables 5a and 5b. The CCC specimens were clearly divided from non-CCC samples based on the expression levels of these genes. The CCC-specific UM genes from our analysis were enriched among a distinct cluster of genes that are highly expressed in the CCC clinical specimens when compared to the presence of CCC-specific HM genes in this cluster (16 of 30 *versus* 0 of 378 in GSE6008, and 18 of 30 *versus* 1 of 378 in GSE2109; $p < 0.0001$ for both; Supporting Information Figs. 4a and 4b).

Validation of hypermethylation and decreased expression of estrogen receptor pathway genes in CCC

Representative ER pathway genes including *ESR1, BMP4, DKK1, SOX11, SNCG* and *MOSC1* were investigated for their methylation status in cell lines using MS-PCR. Twelve of 14 (86%) CCC cell lines exhibited methylation of the *ESR1* promoter, whereas 17 of 32 (53%) non-CCC cell lines showed methylation of this gene ($p = 0.0487$). Similarly, more of the CCC *versus* non-CCC cell lines showed methylation at the *BMP4* and *DKK1* promoter regions (*BMP4*: 12 of 14 CCCs *versus* 8 of 32 non-CCCs, $p = 0.0002$; *DKK1*: 10 of 14 CCCs *versus* 9 of 32 non-CCCs, $p = 0.0094$; Table 2, top and Supporting Information Figs. 5a–5f). For *SOX11* and *SNCG*, all CCC cell lines exhibited methylation while there were several non-CCC unmethylated cell lines (*SOX11*: 13 of 13 CCCs *versus* 18 of 23 non-CCCs, $p = 0.1363$; *SNCG*: 13 of 13 CCCs *versus* 21 of 24 non-CCCs, $p = 0.5382$). The *MOCS1* gene showed evidence of methylation in all cell lines

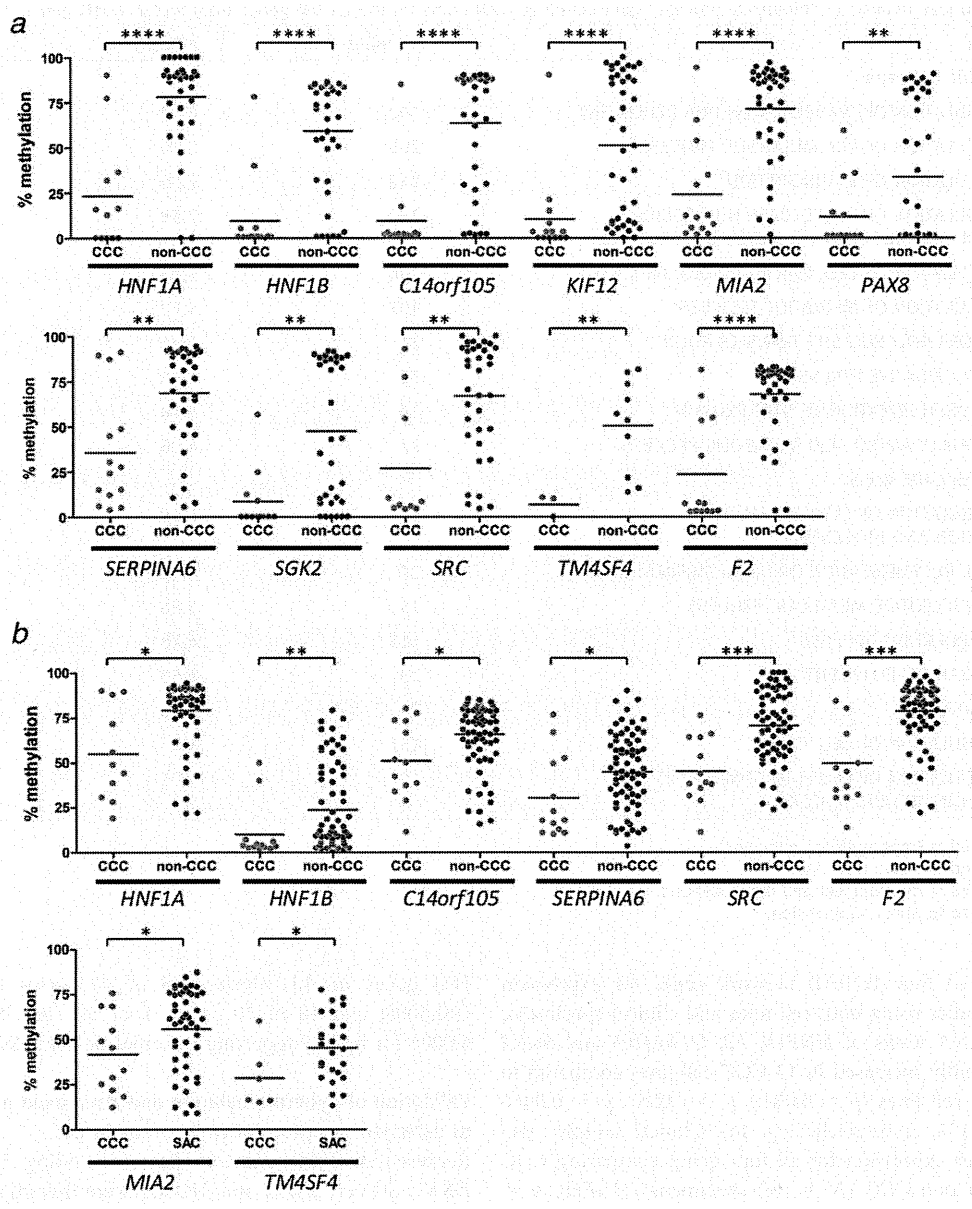

Figure 3. Quantitative methylation analyses of 11 HNF1 network genes (*HNF1A, HNF1B, C14orf105, KIF12, MIA2, PAX8, SERPINA6, SGK2, SRC, TM4SF4* and *F2*) in cell lines by bisulfite pyrosequencing show lower levels of methylation in CCC *versus* non-CCC, supporting the results from the Infinium BeadChip (*a*). For clinical specimens, six of 11 HNF1 network genes show significantly decreased methylation in CCC compared to non-CCC. When CCC is compared with SAC in clinical samples, eight genes (*HNF1A*, $p = 0.0007$; *HNF1B*, $p = 0.0002$; *C14orf105*, $p = 0.0073$; *SERPINA6*, $p = 0.0071$; *SRC*, $p < 0.0001$ and *F2*, $p < 0.0001$, included in data shown in Fig. 3*b*, top; *MIA2*, $p = 0.0480$ and *TM4SF4*, $p = 0.0452$ are shown below) are significantly hypomethylated in CCC (*b*). $^{*}p \leq 0.05$, $^{**}p \leq 0.01$, $^{***}p \leq 0.001$, $^{****}p \leq 0.0001$.

analyzed. We also investigated these six genes in clinical specimens, and three of the six (*SOX11, BMP4* and *MOCS1*) were methylated more often in CCC than in non-CCC, with *SOX11* showing a significant difference ($p = 0.0116$) and *BMP4* and *MOCS1* approaching significance ($p = 0.0645$ and 0.1784, respectively; Table 2, bottom and Supporting Information Figs. 6a–6f).

Transcript levels for five ER pathway genes (*ESR1, CRIP1, SOX11, IGFBP4* and *BMP4*) were decreased in CCC cell lines when compared to non-CCC cell lines, all of which were significant except for *SOX11* ($p = 0.0112$, $p = 0.0046$, $p = 0.2108$, $p = 0.0038$ and $p = 0.0472$, respectively; Fig. 4*a*). Among the clinical specimens, four genes showed lower average expression levels in CCC compared to non-CCC, with a

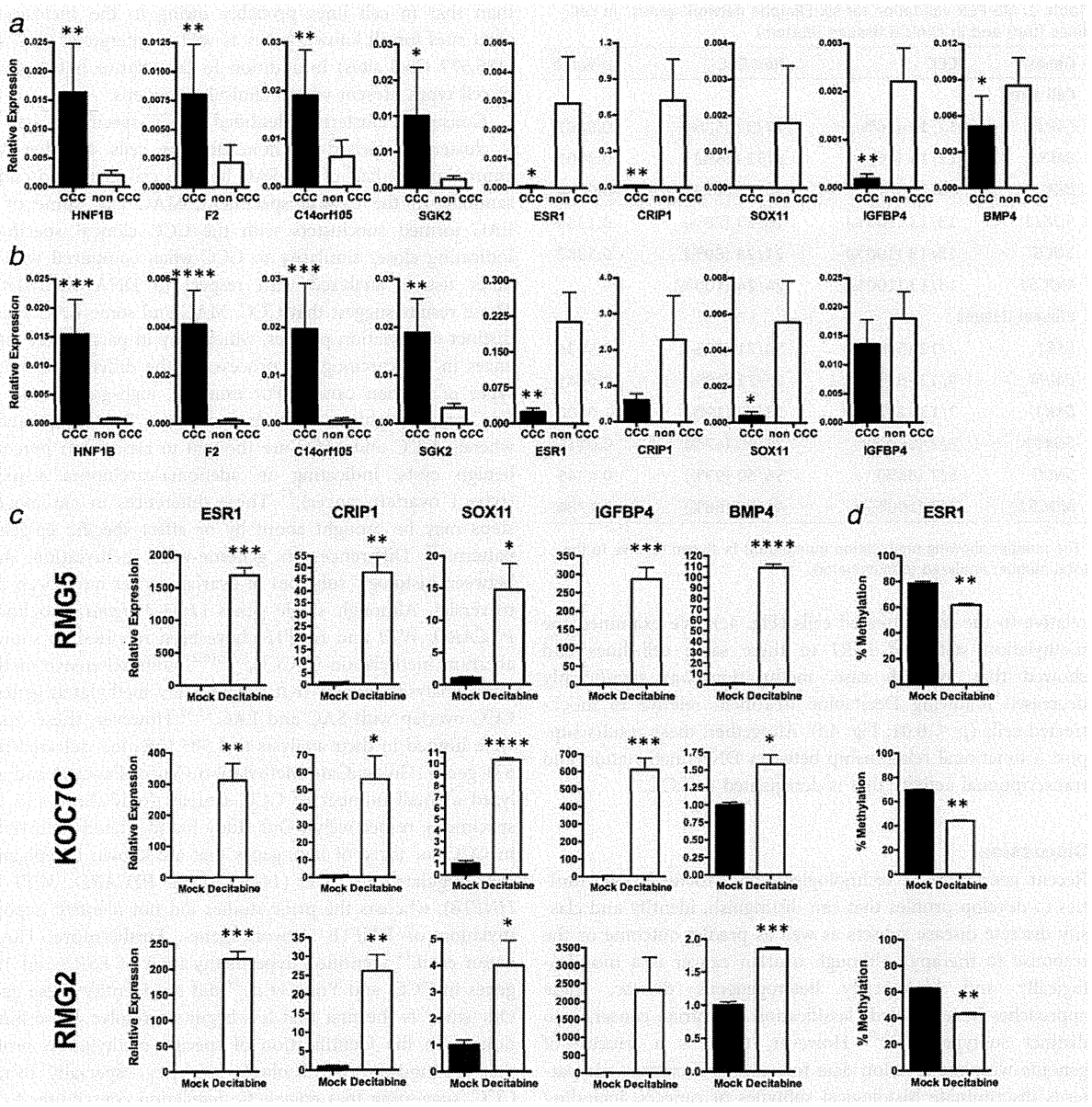

Figure 4. Validation of altered expression of HNF1 network and ERalpha pathway genes in CCC and reactivation and demethylation of ERalpha pathway genes with 5-aza-2′-deoxycytidine (Decitabine) treatment. Quantitative RT-PCR of HNF1 network genes (*HNF1A, F2, C14orf105* and *SGK2*) and ERalpha pathway genes (*ESR1, CRIP1, SOX11, IGFBP4* and *BMP4*) using cell lines (*a*) and clinical samples (*b*). The expression of ERalpha pathway genes (*ESR1, CRIP1, SOX11, IGFBP4* and *BMP4*) is markedly induced by demethylating agent Decitabine in three CCC cell lines (RMG-5, KOC-7C and RMG-2) (*c*). Methylation at the *ESR1* promoter is decreased in response to Decitabine treatment (*d*). $^{*}p \leq 0.05$, $^{**}p \leq 0.01$, $^{***}p \leq 0.001$, $^{****}p \leq 0.0001$.

significant difference for two (*ESR1*, $p = 0.0014$; *CRIP1*, $p = 0.1853$; *SOX11*, $p = 0.0476$ and *IGFBP4*, $p = 0.991$; Fig. 4*b*). When compared to SAC, *IGFBP4* mRNA levels did not differ in CCC ($p = 0.9521$), but expression of *ESR1*, *CRIP1* and *SOX11* was significantly decreased in CCC ($p = 0.0022$, $p = 0.0476$ and $p = 0.0017$, respectively).

The potential to reactivate expression of five genes, *ESR1*, *CRIP1*, *SOX11*, *IGFBP4* and *BMP4*, was evaluated in three CCC cell lines (RMG-2, RMG-5 and KOC-7C) using the DNA methyltransferase inhibitor, 5-aza-2′-deoxycytidine (Decitabine). There was a marked and significant increase in mRNA levels for all five genes in cells treated with Decitabine

Table 2. MS-PCR validation for six ERalpha network genes[1] in cell lines (top) and in clinical tissues (bottom)

Genes	CCC	Non-CCC	*p*-Value
Cell lines			
ESR1	12/14 (86%)	17/32 (53%)	0.0487
BMP4	12/14 (86%)	8/32 (25%)	0.0002
DKK1	10/14 (71%)	9/32 (28%)	0.0094
SOX11	13/13 (100%)	18/23 (78%)	0.1363
SNCG	13/13 (100%)	21/24 (89%)	0.5382
MOCS1	13/13 (100%)	24/24 (100%)	–
Clinical tissues			
ESR1	7/12 (58%)	50/71 (70%)	0.5034
BMP4	9/13 (69%)	27/71 (38%)	0.0645
DKK1	2/13 (15%)	13/70 (19%)	1.0000
SOX11	7/7 (100%)	28/60 (47%)	0.0116
SNCG	6/7 (86%)	56/60 (93%)	0.4345
MOCS1	7/7 (100%)	41/60 (68%)	0.1784

[1]The number showing methylation (numerator) is shown relative to the total number analyzed (denominator).

relative to the mock-treated cells (Fig. 4*c*). We examined the methylation status of *ESR1* in these same cell lines and showed that in each case, methylation was significantly decreased following Decitabine treatment relative to mock-treated cells ($p \leq 0.01$; Fig. 4*d*). Altogether, these results support a functional relationship between DNA methylation and transcriptional activity that is deregulated in CCC.

Discussion

Recent genome-wide technologies have provided opportunities to develop profiles that can distinguish, identify and classify discrete disease subsets as well as predict outcome or the response to therapy. Although ovarian cancer is a morphologically and biologically heterogeneous disease, these approaches have enabled classification of ovarian cancers into distinct subtypes.[2,31,33,34] However, there is a paucity of genome-wide methylation data to examine if epigenomic patterns discriminate histological subtypes of cancers, including ovarian cancer.

The comparison of methylation profiles between ovarian cancer and noncancerous cells indicated that of the 2,003 genes that showed differential levels of methylation, as many as 93.4% showed hypermethylation in the cancer cell lines. Based on prior focused studies of promoter CpG island methylation and next-generation sequencing, acquisition of methylation occurs more frequently than loss of methylation in almost all types of primary tumors when compared to their normal counterparts.[35,36] Because 26,956 (97.7%) of the 27,578 CpG sites are located at promoter regions on the Illumina Infinium HumanMethylation27 BeadChip, our results are comparable with those of published reports. The ratio of HM genes (65.5%) in primary cancer tissues was smaller than that in cell lines probably owing to the inclusion of CpG sites for all known genes as well as intergenic CpG sites (485,577 CpG sites) in addition to the relative heterogeneity of cell types present within clinical specimens.

Consensus clustering identified a CCC-specific cluster and a cluster comprised of noncancerous cells together with approximately half of the SAC both in cell lines and clinical samples. In the clinical specimens, MAC and some of the EAC formed subclusters with the CCC clinical specimens, indicating closer similarity to CCC when compared with the other tissues analyzed with respect to DNA methylation. These results suggest that CCC, MAC and some EAC acquire distinct methylation profiles, which may in part reflect differences in the carcinogenic process for the different histologic types of ovarian cancer. For example, high-grade SAC and EAC are thought to arise *de novo* (type 2 ovarian cancer), whereas CCC and MAC are thought to arise from precursor benign cysts, indicating an adenoma-carcinoma sequence (type 1 ovarian cancer).[37] These differences in carcinogenic steps may be brought about by or affect specific epigenetic patterns.[38] Differences in genome-wide methylation status between histologic subtypes of ovarian cancer have been controversial. Although single genes (*14-3-3 sigma* also known *PYCARD, WT1* and *HNF1B*) have been reported as showing aberrant methylation in CCC,[1,13,16,21] comprehensive methylation analyses showed that differentially methylated genes in CCC overlap with SAC and EAC.[14,39] However, these studies were limited in their analysis to 1,505 CpG loci selected from 871 genes (GoldenGate Methylation Cancer Panel I) and analyzed a small number of CCC samples (only three and four specimens, respectively). Our study found altered methylation in CCC for three of four genes that are known as epigenetically regulated in CCC (*14-3-3 sigma PYCARD, WT1* and *HNF1B*), whereas the prior studies did not identify hypomethylation of HNF1B network genes. Furthermore, Houshdaran *et al.*[14] identified hypermethylation of *ESR1* and *WT1* genes in CCC, and Yoon *et al.*[39] did not identify these genes. Our study is the first that has begun to resolve these limitations with the identification of specific methylation profiles that distinguish the histologic subtypes, especially ovarian CCC, suggesting that epigenetic regulation contributes to the ontogeny of epithelial ovarian cancer.

Although many single genes have been reported as regulated by DNA methylation in ovarian cancer, the biological role of genome-wide methylation in ovarian carcinogenesis has not been elucidated, with questions remaining as to whether or not changes in methylation reflect cause or consequence. We considered the genes showing an inverse correlation between expression and methylation as functionally important genes that are regulated at least in part through epigenetic mechanisms. For our purposes, the data from cell lines were used to evaluate expression-methylation correlations and proved more powerful at revealing these relationships than the clinical samples, likely because of the heterogeneity in cell type composition of the clinical tissue

specimens and because the DNA and RNA were extracted from different parts of the same piece of tissue. Therefore, to analyze how DNA methylation influences biological features of CCC, we identified genes for which transcription and methylation are coordinately related and that are CCC-specific. Interestingly, our pathway and categorical analyses showed that genes with HNF1 transcription factor-binding sites as well as *HNF1B* were synchronously hypomethylated in CCC. Furthermore, genes that function in the ERalpha network in CCC were among the 276 HM genes, including *ESR1* and *WT1*. These findings suggest that hypomethylation and hypermethylation in CCC appear to target genes belonging to specific and highly relevant pathways in this particular histologic subtype of ovarian cancer.

Previously, we reported that HNF1 transcription is activated in CCC relative to the other ovarian cancer histologic subtypes, and this activation is related to loss of DNA methylation at *HNF1B*.[13,21,40] Our finding that activation occurs of multiple components of the HNF1 pathway by synchronous hypomethylation is a significant step forward in understanding this process and supports previous studies. HNF1B is involved in glucose homeostasis and may be responsible for the prominence of glycogen in CCC cells[41,42] causing the cytoplasm to be clear in appearance, a defining feature of CCC. Our findings suggest that this morphologic feature of CCC is at least in part epigenetically regulated. Ovarian CCC is characterized by unique biology, including slow growth and resistance to chemotherapy and oxidative stress. Ovarian CCC also exhibits the molecular phenotypes of HNF1 pathway activation, PI3K pathway activation and MAPK activation, traits that have been collectively referred to as "ovarian CCC-likeness."[4] Using GO term analysis, CCC-specific UM genes were enriched with genes related to oxidative stress, consistent with "ovarian CCC-likeness." These results indicate that loss of DNA methylation appears to target specific pathways and biological functions, with hypomethylation influencing pathways that help sculpt the characteristic biology of the disease.

ESR1, which is a key molecule in the ERalpha network that we found is hypermethylated in ovarian CCC, is a known target of methylation, and the absence of ERalpha expression in CCC has been reported.[43–45] *WT1*, one of the genes regulated by ERalpha signaling, has previously been shown to be inactivated by promoter methylation in ovarian CCC.[46] These results support our findings and underscore the importance of epigenetic regulation of this pathway in CCC. Endometriotic cysts of the ovary are precursors of ovarian cancer, especially of the CCC and EAC histologic subtypes.[4] Akahane *et al.* showed that reductions in ERalpha expression occurred with progression from endometriosis to atypical endometriosis in CCC specimens, whereas ERalpha expression increased with malignant transformation in EAC.[47] Estrogen signaling through estrogen receptors has divergent outcomes in that it can induce activation of cell proliferation but also inhibit cell cycle progression.[48,49] Our results indicate that the ERalpha signaling-independent growth of CCC is largely attributable to aberrant epigenetic alterations in CCC. Although changes in CCC phenotype cannot be specifically assessed using demethylating agents, these findings support our hypothetical model for the malignant transformation of endometriosis, in which EAC is induced by estrogen and CCC is influenced by the unique microenvironment within endometriotic cysts, including persistent exposure to oxidative stress and chronic inflammation.[4] Epigenetic changes can be the earliest initiation factor and complement single driver mutations in a human cancer;[50] our results suggest that coordinate deregulation of DNA methylation leads not only to tumor development but also defines the biological features of the malignancy.

We previously reported suppression of TGFbeta pathway activity by DNA methylation in ovarian cancers, primarily of serous histology,[26] while our study demonstrates that there are distinct pathways influenced by hypomethylation and hypermethylation in ovarian CCC. Genetic and epigenetic disruption plays a fundamental role in cancer development. However, mutations in *ARID1A* and *PIK3CA* are the only genetic alterations that have been identified in ~50% and 40% of CCC cases, respectively. Thus, gene mutations alone cannot distinguish histologic subtypes of ovarian cancer. Our results indicate that coordinate changes in DNA methylation occur that affect expression of genes belonging to specific and relevant pathways in ovarian CCC, which contrasts with the more isolated pattern of genetic mutations observed in this disease. In high-grade SAC, *TP53* mutations initiate carcinogenesis and also contribute to the rapid growth that characterizes this histologic subtype, a "genetically based disposition." On the other hand, *ARID1A* mutations lead to malignant transformation from endometriosis to CCC and the specific biological characteristics of CCC and "ovarian CCC-likeness" are developed through alteration of DNA methylation, an "epigenetically based disposition." Furthermore, although changes in methylation levels induced by environmental stress such as oxidative stress and inflammation were not analyzed in this study, our current and prior results collectively suggest that CCC tumor development is brought about by microenvironment-mediated effects resulting from oxidative stress that lead to these CCC-specific methylation profiles.[13] Inflammatory diseases such as ulcerative colitis and chronic gastritis resulting from *Helicobacter pylori* infection induce increased DNA methylation and are associated with increased cancer risk.[51] Together, these findings suggest that an "epigenetically based disposition" may be involved in inflammation-induced carcinogenesis.

In summary, our genome-wide methylation analyses have revealed that ovarian CCC has a distinct methylation profile relative to the other histological subtypes of epithelial ovarian cancer. The CCC-specific methylation profile includes synchronous gain of promoter methylation for multiple genes in the ERalpha pathway and loss of promoter methylation for multiple genes in the HNF1 pathway. Further work will be required to more precisely delineate the functions of these

two pathways in this disease, to develop these changes as epigenetic biomarkers and to explore new modalities of treatment for CCC, including epigenetic therapies.

Acknowledgements

The authors thank Carole Grenier and Darby Kroyer for excellent technical assistance.

References

1. Barton CA, Hacker NF, Clark SJ, et al. DNA methylation changes in ovarian cancer: implications for early diagnosis, prognosis and treatment. *Gynecol Oncol* 2008;109:129–39.
2. Gomez-Raposo C, Mendiola M, Barriuso J, et al. Molecular characterization of ovarian cancer by gene-expression profiling. *Gynecol Oncol* 2010; 118:88–92.
3. Cho KR, Shih Ie M. Ovarian cancer. *Annu Rev Pathol* 2009;4:287–313.
4. Mandai M, Yamaguchi K, Matsumura N, et al. Ovarian cancer in endometriosis: molecular biology, pathology, and clinical management. *Int J Clin Oncol* 2009;14:383–91.
5. Skirnisdottir I, Seidal T, Karlsson MG, et al. Clinical and biological characteristics of clear cell carcinomas of the ovary in FIGO stages I-II. *Int J Oncol* 2005;26:177–83.
6. Sugiyama T, Kamura T, Kigawa J, et al. Clinical characteristics of clear cell carcinoma of the ovary: a distinct histologic type with poor prognosis and resistance to platinum-based chemotherapy. *Cancer* 2000;88:2584–9.
7. Itamochi H, Kigawa J, Terakawa N. Mechanisms of chemoresistance and poor prognosis in ovarian clear cell carcinoma. *Cancer Sci* 2008;99:653–8.
8. Chan JK, Teoh D, Hu JM, et al. Do clear cell ovarian carcinomas have poorer prognosis compared to other epithelial cell types?. A study of 1411 clear cell ovarian cancers. *Gynecol Oncol* 2008;109:370–6.
9. Ricciardelli C, Oehler MK. Diverse molecular pathways in ovarian cancer and their clinical significance. *Maturitas* 2009;62:270–5.
10. Wiegand KC, Shah SP, Al-Agha OM, et al. *ARID1A* mutations in endometriosis-associated ovarian carcinomas. *N Engl J Med* 2010;363: 1532–43.
11. Jones S, Wang TL, Shih Ie M, et al. Frequent mutations of chromatin remodeling gene *ARID1A* in ovarian clear cell carcinoma. *Science* 2010;330: 228–31.
12. Tsuchiya A, Sakamoto M, Yasuda J, et al. Expression profiling in ovarian clear cell carcinoma: identification of hepatocyte nuclear factor-1 beta as a molecular marker and a possible molecular target for therapy of ovarian clear cell carcinoma. *Am J Pathol* 2003;163:2503–12.
13. Yamaguchi K, Mandai M, Oura T, et al. Identification of an ovarian clear cell carcinoma gene signature that reflects inherent disease biology and the carcinogenic processes. *Oncogene* 2010; 29:1741–52.
14. Houshdaran S, Hawley S, Palmer C, et al. DNA methylation profiles of ovarian epithelial carcinoma tumors and cell lines. *PLoS One* 2010;5: e9359.
15. Gargiulo G, Minucci S. Epigenomic profiling of cancer cells. *Int J Biochem Cell Biol* 2009;41:127–35.
16. Asadollahi R, Hyde CA, Zhong XY. Epigenetics of ovarian cancer: from the lab to the clinic. *Gynecol Oncol* 2010;118:81–7.
17. Wei SH, Balch C, Paik HH, et al. Prognostic DNA methylation biomarkers in ovarian cancer. *Clin Cancer Res* 2006;12:2788–94.
18. Kamalakaran S, Kendall J, Zhao X, et al. Methylation detection oligonucleotide microarray analysis: a high-resolution method for detection of CpG island methylation. *Nucleic Acids Res* 2009; 37:e89.
19. Wei SH, Chen CM, Strathdee G, et al. Methylation microarray analysis of late-stage ovarian carcinomas distinguishes progression-free survival in patients and identifies candidate epigenetic markers. *Clin Cancer Res* 2002;8: 2246–52.
20. Ahluwalia A, Yan P, Hurteau JA, et al. DNA methylation and ovarian cancer. I. Analysis of CpG island hypermethylation in human ovarian cancer using differential methylation hybridization. *Gynecol Oncol* 2001;82:261–8.
21. Terasawa K, Toyota M, Sagae S, et al. Epigenetic inactivation of *TCF2* in ovarian cancer and various cancer cell lines. *Br J Cancer* 2006;94: 914–21.
22. Maeda T, Tashiro H, Katabuchi H, et al. Establishment of an immortalised human ovarian surface epithelial cell line without chromosomal instability. *Br J Cancer* 2005;93:116–23.
23. Maines-Bandiera SL, Kruk PA, Auersperg N. Simian virus 40-transformed human ovarian surface epithelial cells escape normal growth controls but retain morphogenetic responses to extracellular matrix. *Am J Obstet Gynecol* 1992; 167:729–35.
24. Auersperg N, Maines-Bandiera SL, Dyck HG, et al. Characterization of cultured human ovarian surface epithelial cells: phenotypic plasticity and premalignant changes. *Lab Invest* 1994;71: 510–18.
25. Seiler M, Huang CC, Szalma S, et al. ConsensusCluster: a software tool for unsupervised cluster discovery in numerical data. *OMICS* 2010;14: 109–13.
26. Matsumura N, Huang Z, Mori S, et al. Epigenetic suppression of the TGF-beta pathway revealed by transcriptome profiling in ovarian cancer. *Genome Res* 2011;21:74–82.
27. Johnson WE, Li C, Rabinovic A. Adjusting batch effects in microarray expression data using empirical Bayes methods. *Biostatistics* 2007;8: 118–27.
28. Subramanian A, Tamayo P, Mootha VK, et al. Gene set enrichment analysis: a knowledge-based approach for interpreting genome-wide expression profiles. *Proc Natl Acad Sci USA* 2005;102: 15545–50.
29. Newton MA, Quintana FA, den Boon JA, et al. Random-set methods identify distinct aspects of the enrichment signal in gene-set analysis. *Ann Appl Stat* 2007;1:85–106.
30. Pyeon D, Newton MA, Lambert PF, et al. Fundamental differences in cell cycle deregulation in human papillomavirus-positive and human papillomavirus-negative head/neck and cervical cancers. *Cancer Res* 2007;67: 4605–19.
31. Marquez RT, Baggerly KA, Patterson AP, et al. Patterns of gene expression in different histotypes of epithelial ovarian cancer correlate with those in normal fallopian tube, endometrium, and colon. *Clin Cancer Res* 2005;11:6116–26.
32. Wu R, Hendrix-Lucas N, Kuick R, et al. Mouse model of human ovarian endometrioid adenocarcinoma based on somatic defects in the Wnt/beta-catenin and PI3K/Pten signaling pathways. *Cancer Cell* 2007;11:321–33.
33. Bell D, Berchuck A, Birrer M, et al. Integrated genomic analyses of ovarian carcinoma. *Nature* 2011;474:609–15.
34. Schwartz DR, Kardia SL, Shedden KA, et al. Gene expression in ovarian cancer reflects both morphology and biological behavior, distinguishing clear cell from other poor-prognosis ovarian carcinomas. *Cancer Res* 2002;62:4722–9.
35. Cheung HH, Lee TL, Rennert OM, et al. DNA methylation of cancer genome. *Birth Defects Res C Embryo Today* 2009;87:335–50.
36. Ruike Y, Imanaka Y, Sato F, et al. Genome-wide analysis of aberrant methylation in human breast cancer cells using methyl-DNA immunoprecipitation combined with high-throughput sequencing. *BMC Genomics* 2010;11:137.
37. Kurman RJ, Shih Ie M. Molecular pathogenesis and extraovarian origin of epithelial ovarian cancer—shifting the paradigm. *Hum Pathol* 2011;42: 918–31.
38. Scott M, McCluggage WG. Current concepts in ovarian epithelial tumorigenesis: correlation between morphological and molecular data. *Histol Histopathol* 2006;21:81–92.
39. Yoon MS, Suh DS, Choi KU, et al. High-throughput DNA hypermethylation profiling in different ovarian epithelial cancer subtypes using universal bead array. *Oncol Rep* 2010;24:917–25.
40. Matsumura N, Mandai M, Okamoto T, et al. Sorafenib efficacy in ovarian clear cell carcinoma revealed by transcriptome profiling. *Cancer Sci* 2010;101:2658–63.
41. Pontoglio M. Hepatocyte nuclear factor 1, a transcription factor at the crossroads of glucose homeostasis. *J Am Soc Nephrol* 2000;11 (Suppl 16):S140–S143.
42. Kobel M, Kalloger SE, Carrick J, et al. A limited panel of immunomarkers can reliably distinguish between clear cell and high-grade serous carcinoma of the ovary. *Am J Surg Pathol* 2009;33: 14–21.
43. Smuc T, Hevir N, Ribic-Pucelj M, et al. Disturbed estrogen and progesterone action in ovarian endometriosis. *Mol Cell Endocrinol* 2009;301: 59–64.
44. Fujimura M, Hidaka T, Kataoka K, et al. Absence of estrogen receptor-alpha expression in human ovarian clear cell adenocarcinoma compared with ovarian serous, endometrioid, and mucinous adenocarcinoma. *Am J Surg Pathol* 2001;25:667–72.
45. Wiley A, Katsaros D, Chen H, et al. Aberrant promoter methylation of multiple genes in malignant ovarian tumors and in ovarian tumors with low malignant potential. *Cancer* 2006;107: 299–308.
46. Kaneuchi M, Sasaki M, Tanaka Y, et al. *WT1* and *WT1-AS* genes are inactivated by promoter meth-

ylation in ovarian clear cell adenocarcinoma. *Cancer* 2005;104:1924–30.
47. Akahane T, Sekizawa A, Okuda T, et al. Disappearance of steroid hormone dependency during malignant transformation of ovarian clear cell cancer. *Int J Gynecol Pathol* 2005;24:369–76.
48. Wright JW, Stouffer RL, Rodland KD. Estrogen inhibits cell cycle progression and retinoblastoma phosphorylation in rhesus ovarian surface epithelial cell culture. *Mol Cell Endocrinol* 2003;208:1–10.
49. Cunat S, Hoffmann P, Pujol P. Estrogens and epithelial ovarian cancer. *Gynecol Oncol* 2004;94:25–32.
50. Baylin SB, Jones PA. A decade of exploring the cancer epigenome—biological and translational implications. *Nat Rev Cancer* 2011;11:726–34.
51. Schetter AJ, Heegaard NH, Harris CC. Inflammation and cancer: interweaving microRNA, free radical, cytokine and p53 pathways. *Carcinogenesis* 2010;31:37–49.

Hepatocyte Nuclear Factor-1β (HNF-1β) Promotes Glucose Uptake and Glycolytic Activity in Ovarian Clear Cell Carcinoma

Takako Okamoto,[1,2] Masaki Mandai,[1]* Noriomi Matsumura,[1] Ken Yamaguchi,[1] Hiroshi Kondoh,[3] Yasuaki Amano,[1] Tsukasa Baba,[1] Junzo Hamanishi,[1] Kaoru Abiko,[1] Kenzo Kosaka,[1] Susan K. Murphy,[2] Seiichi Mori,[4], and Ikuo Konishi[1]

[1]*Department of Gynecology and Obstetrics, Kyoto University Graduate School of Medicine, Kyoto, Japan*
[2]*Department of Obstetrics and Gynecology, Division of Gynecologic Oncology, Duke University Medical Center, Durham, North Carolina*
[3]*Department of Geriatric Medicine, Kyoto University Graduate School of Medicine, Kyoto, Japan*
[4]*Cancer Genomics, Cancer Institute, Japanese Foundation for Cancer Research, Tokyo, Japan*

Ovarian clear cell carcinoma (OCCC) is a morphologically and biologically distinct subtype of ovarian carcinomas that often arises in ovarian endometriosis. We previously reported that a unique carcinogenic environment, especially iron-induced oxidative stress in endometriotic cysts may promote development of OCCC. We also identified a gene expression profile characteristic of OCCC (the "OCCC signature"). This 320-gene OCCC signature is enriched in genes associated with stress response and sugar metabolism. However, the biological implication of this profile is unclear. In this study, we have focused on the biological role of the *HNF-1β* gene within the OCCC signature, which was previously shown to be overexpressed in OCCC. Suppression of HNF-1β in the HNF-1β-overexpressing human ovarian cancer cell line RMG2 using short hairpin RNA resulted in a significant increase in proliferation. It also facilitated glucose uptake, glycolytic activity, and lactate secretion along with increased expression of the glucose transporter-1 (*GLUT-1*) gene and several key enzymes in the glycolytic process. Conversely, forced expression of HNF-1β in the serous ovarian cancer cell line, Hey, resulted in slowed cellular growth and repressed glycolytic activity. These data suggest that HNF-1β represses cell growth, and at the same time, it promotes aerobic glycolysis which is known as the "Warburg effect." As the Warburg effect is regarded as a characteristic metabolic process in cancer which may contribute to cell survival under hypoxic conditions or in a stressful environment, overexpression of HNF-1β may play an inevitable role in the occurrence of OCCC in stressful environment.

Key words: ovarian clear cell carcinoma; HNF1β; glucose metabolism

INTRODUCTION

Ovarian cancer is the leading cause of death among gynecological malignancies. Epithelial ovarian cancer consists of four histologically distinct subtypes, namely, serous, mucinous, endometrioid, and clear cell carcinoma. Ovarian clear cell carcinoma (OCCC) has distinct clinical features as compared to other subtypes: it is generally chemo-resistant, is often accompanied by a thromboembolic complications, and shows slow growth but with unfavorable outcomes. The most notable feature of OCCC is its relationship with ovarian endometriosis. According to epidemiological surveys, approximately 1% of ovarian endometriosis eventually transforms into carcinoma, primarily of the clear cell and endometrioid subtypes. This strongly suggests that there is a specific carcinogenic trajectory that directs the malignant transformation of endometriosis [1–6].

We previously reported that the unique composition of endometriotic cyst fluid, especially the high free iron concentration, promotes carcinogenesis through persistent oxidative stress [7]. We also identified a microarray-based gene signature that is specific to OCCC, which we designated as the "OCCC signature." Analyses of the OCCC signature revealed that OCCC-specific gene expression is characterized by the involvement of many stress-related genes, which further supports the association between OCCC and stress. Pathway analysis of the OCCC signature demonstrated that an intracellular signaling pathway consisting of a large number of genes, especially stress-related genes, is activated in OCCC. A second prominent gene category overrepresented in

Abbreviations: OCCC, ovarian clear cell carcinoma; *HNF-1β*, hepatic nuclear factor-1β gene; shRNA, short hairpin RNAs; qRT-PCR, quantitative real-time polymerase chain reaction; GSEA, gene set enrichment analysis

All the authors have no conflict of interest to declare regarding this manuscript.

*Correspondence to: 54, Kawaharacho, Shogoin, Sakyo ku, Kyoto 606-8507.

Received 15 February 2013; Revised 25 June 2013; Accepted 1 July 2013

DOI 10.1002/mc.22072

Published online in Wiley Online Library (wileyonlinelibrary.com).

the OCCC signature is metabolism-related, in particular glycogen-related genes, suggesting that OCCC has a distinct metabolic character among the ovarian carcinomas [8]. In this context, our next goal was to characterize the genes responsible for this unique expression profile and define the function of these genes, which may then provide the basis for development of targeted molecular therapy that is specific for OCCC. In this study, we have chosen to focus on a specific OCCC signature gene, hepatic nuclear factor-1β gene (*HNF-1β*).

HNF-1β is a homeodomain-containing transcription factor that shares >80% amino acid sequence of homeodomain [9] homology with HNF-1α. These proteins dimerize and bind to the same DNA sequence as homodimers or heterodimers, and are known to regulate the expression of multiple genes through direct or indirect mechanisms [9]. Clinically, *HNF-1* mutations are responsible for "maturity-onset diabetes of the young (MODY)," a specific type of diabetes characterized by pancreatic hypoplasia. Diabetes has been reported in 58% of *HNF-1β* mutation carriers [10]. HNF-1β has been implicated in the development of the pancreas and is thought to be an essential regulator of the transcriptional network that controls pancreatic morphogenesis and the differentiation of pancreatic endocrine cells [11].

Tsuchiya et al. recently reported that HNF-1β is overexpressed in OCCC. Although they identified an anti-apoptotic effect of this gene, the precise mechanism and biological significance of HNF-1β in OCCC are not yet clear [12]. We have shown that HNF-1β is not only a component of the OCCC signature [8], but also included in the intracellular signaling network demonstrated by pathway analysis, suggesting that this gene plays an important role in the biology of OCCC [13]. Therefore, using HNF-1β knockdown in OCCC cells and HNF-1β overexpression in non-OCCC cells, we report herein elucidation of how HNF-1β functionally plays a role in the unique biology of OCCC from multiple point of view including cell proliferation, glucose metabolism and gene expressions.

MATERIALS AND METHODS

Cell Lines and Cell Culture

The OCCC cell lines, RMG1 and RMG2, and the serous carcinoma cell line, Hey, were cultured in RPMI1640 (Nikken, Kyoto, Japan) supplemented with 10% FBS in a humidified atmosphere containing 5% CO_2 at 37°C, as previously described [8].

Stable Knockdown and Overexpression of the *HNF-1β* Gene

Two *HNF-1β*-targeting short hairpin RNAs (shRNA; clone IDs: V2LHS_204881 and V2LHS_196459) and a non-silencing control (clone ID: RHS4348) were purchased from the GIPZ lentiviral shRNAmir library (Thermo Fisher Scientific, Huntsville, AL). RMG2 cells were infected with lentiviruses using a standard protocol using puromycin as the selective marker. RMG2 cells stably transfected with clones V2LHS_204881 or V2LHS_196459 were designated as RMG2-HNFβ-sh1 and RMG2-HNF1β-sh2, respectively, while RMG2 cells transfected with the non-silencing control were designated as RMG2-control. HNF-1β-suppressed stable cells in RMG1 cell line were established using same method above and designated as RMG1-HNF1β-sh1 while non-silencing control cells were designed as RMG1-control. For HNF-1β-overexpressing cell line, an HNF-1β-expressing lentivirus was constructed using an entry vector, pENTR221, containing the HNF-1β cDNA (Cat. No. OHS4559-99857765a; Thermo Fisher Scientific), and a destination vector, pLenti6/V5-DEST, in a Gateway system (Invitrogen Japan, Tokyo, Japan). Hey cells were infected with the HNF-1β-expressing lentivirus and were selected with blasticidin (Hey-HNF1β). The Hey cells transfected with an empty lentiviral vector were used as a control (Hey-control).

RNA Extraction and Quantitative Real-Time Polymerase Chain Reaction (qRT-PCR)

Total RNA was isolated from cells at 80% confluency using the RNeasy Mini Kit (Qiagen, Tokyo, Japan). Quantitative RT-PCR (qRT-PCR) was performed with primers and probe specific for *HNF-1β* (Assay ID: Hs00172123_ml) and *SOD1* (Assay ID: Hs00533490_m1; Taqman Gene Expression Assays; Applied Biosystems, Foster City, CA). All other assays were designed using Roche Probefinder software at the Universal Probe Library Assay Design Center (https://www.roche-applied-science.com/sis/rtpcr/upl/index.jsp?id=UP030000). Primer and probe sequences are provided in Supplementary Table 1. The samples were analyzed using a LightCycler 480 Real-Time PCR system (Roche Diagnostics, Tokyo, Japan).

Protein Extraction and Western Blot Analysis

Protein extraction and Western blotting were performed as reported previously [13] using the following primary antibodies: anti-HNF-1β (1:200; Santa Cruz, CA), anti-CDKN1B (1:1000, BD Bioscience, Franklin Lakes, NJ), anti-CDKN1A (1:200; Santa Cruz, CA), anti-GLUT1 (1:2500, Abcam Plc, Cambridge, UK), and anti-β-Actin (1:5000, Abcam Plc). Horseradish peroxidase-linked secondary antibodies were as follows: anti-goat Ig for HNF-1β (1:10 000, DAKO, Glostrup, Denmark) and CDKN1A (1:3000, GE Healthcare, Buckinghamshire, UK), anti-mouse Ig for CDKN1B (1:1000, GE Healthcare) and GAPDH (1:1000, Santa Cruz, CA), anti-rabbit Ig for GLUT1 and β-actin (1:2500 and 1:10 000, respectively, GE Healthcare). Images were obtained using a ChemiDoc XRS Plus system (Bio-Rad Laboratories, Tokyo, Japan).

Proliferation Assays

Cells were seeded into 96-well (2.5×10^3 cells/well) tissue culture plates and incubated for 3 d. Cell numbers were counted at three consecutive time points using a WST-8 (Water Soluble Tetrazolium salts) assay kit, which is a modified MTT (3-(4,5-di-methylthiazol-2-yl)-2,5-diphenyltetrazolium bromide) assay (Nakalai tesque, Kyoto, Japan). WST-8 assay values were normalized using the WST-8 value at the initial time point (Day 0), and compared between the groups. Population doubling times (PDT) were calculated based on the slope angle of the linear regression model for the three time points. In addition to WST-8 assays, cell numbers were directly counted in sextuplicate using the Countess Automated cell counter (Invitrogen) after the cells were seeded into 6-well tissue culture plates (3.0×10^5 cells/well) and incubated for 2, 5, and 11 d. The values were normalized at the initial time point (Day 0) same as above.

The Cell Cycle Analysis

The cell cycle analysis was performed as described previously [14]. The cells (1×10^6/well) were seeded in 10 cm^2 tissue culture dishes and cultured. The next day, cells were treated by nocodazole (Sigma–Aldrich, St. Louis, MO) at a final concentration of 0.5 μg/mL. After incubation for 0, 12, 24 h, cells were fixed with 70% ethanol, stained with 25 μg/mL propidium iodide (Sigma–Aldrich) and analyzed by FACS-Calibur flow cytometry with Cell Quest software (Becton Dickson, Franklin Lakes, NJ). For analysis of S-phase cell, cells were pulse-labeled with 10 μM BrdU for 1 h, fixed with 70% ethanol, denatured, and stained with APC conjugated Anti-BrdU Antibody (Becton Dickson), according to manufacturer's instructions.

Glucose Uptake Assay and Measurement of Lactate Production

Glucose uptake assays were performed as reported previously [15]. In brief, cells were incubated with glucose-free medium with 1 μCi 2-deoxy-[^{3}H]-D-glucose for 60 min. The cells were then washed three times with ice-cold PBS, collected, and quantified using a liquid scintillation counter. Lactate production was evaluated by measuring the concentration in the medium after 24 h of incubation. The assay was performed in triplicate, repeated three times and all the values were normalized by total protein concentration.

Glycolytic Flux Measurement

Measurement of glycolytic flux was performed as reported previously [16]. In brief, $0.7–3.0 \times 10^6$ cells were plated in a 10 cm^2 dish. The medium was changed the following day to a low-glucose (4.25 mmol/L) medium, and 12 h later, D-[3-^{3}H] glucose (3.6 μCi) was added. Every 2 h, 400 μL of the medium was taken for perchloric acid precipitation. The supernatant was applied to DOWEX 1×8 200–400 MESH Cl resin (Sigma–Aldrich Japan) after dilution in sodium tetraborate. The assay was performed in triplicate, repeated three times and the values were normalized by total protein concentration.

Glucose Uptake After Knockdown of GLUT1 in RMG2 Cells

GLUT1-specific siRNAs (Gene Solution siRNA, Cat. No. SI03089401 and No. SI00089264; Qiagen, Valencia, CA) and a negative-control siRNA (AllStars Negative Control siRNA; Qiagen) were transfected into RMG2 cells using HiPerFect Transfection Reagent (Qiagen). After 48 h incubation for with the siRNAs, glucose uptake assays were performed as described above. To confirm downregulation of *GLUT1* expression, qRT-PCR and Western blotting were performed as described above.

Microarray Analysis

RNA preparation and microarray analysis were performed as described [8,13]. Genome set Human U133 Plus 2.0 chips (Affymetrix, Santa Clara, CA) were used and expression of HNF-1β-knockdown and non-silencing control cells were compared using replicate cell preparations (five replicates each for RMG2-HNF1β-sh1 and RMG2-HNF1β-sh2, ten replicates for the RMG2-control). The enrichment of the OCCC signature in control (non-silencing) cells versus HNF-1β-knockdown cells was evaluated using Gene Set Enrichment Analysis (http://www.broadinstitute.org/gsea/index.jsp; GSEA). GSEA is a tool to determine if a particular set of pre-defined genes is over- or under-represented in a given sample. Here, probe sets that were previously shown [8] to be upregulated (n = 393) and downregulated (n = 44) were analyzed in RMG2 cells following knockdown of HNF-1β using two independent shRNAs. Interpretation of output figures is described in detail in the GSEA website (http://www.broadinstitute.org/gsea/index.jsp). Bayesian binary regression 2.0 (http://data.genome.duke.edu/oncogene.php) was used to calculate the HNF-1β signature probability scores of cells, indicating transcriptional pathway activity of HNF-1β downstream genes. Published microarray dataset GSE6008 (consisting of data from 8 OCCC and 91 non-OCCC specimens) was obtained from the Gene Expression Omnibus (GEO) website (http://www.ncbi.nlm.nih.gov/geo/). The GSE2109 dataset was also obtained from the GEO website, and 16 OCCC and 184 non-OCCC (excluding borderline tumors) were used for this analysis. Cell lines used in the present study are listed in Supplementary Table 2.

Statistical Analysis

Differences between groups were assessed using two-tailed unpaired *t*-tests. Data are represented

as mean ± standard deviation (SD). Statistical analysis was performed using GraphPad Prism 4 software (GraphPad Software, Inc., La Jolla, CA), and probability values below 0.05 were considered as significant.

RESULTS

Effect of HNF-1β Knockdown on In Vitro Cell Proliferation

Expression of *HNF-1β* mRNA in shRNA-transfected cells was evaluated using qRT-PCR. *HNF-1β* expression was significantly suppressed (% suppression is 87.3% in RMG2-HNF1β-sh1 ($P=0.009$) and 71.6% in RMG2-HNF1β-sh2 ($P=0.013$) compared with the RMG2-control cells (Figure 1A). Suppression of HNF-1β protein was also confirmed by Western blot (Figure 1A).

Silencing of HNF-1β was associated with an increase in cell proliferation in RMG2 cells as detected using WST-8 assays ($P<0.01$; Figure 1B) and based on cell counts ($P<0.0001$; Figure 1B). PDT of RMG2-HNF1β-sh1, RMG2-HNF1β-sh2, and RMG2-control cells were 27.2, 21.5, and 34.5 h, respectively, as assessed by WST-8 assays, and were 1.94, 1.43, and 2.37 d, respectively, based on direct cell counts.

The suppression of HNF-1β in another OCCC cells, RMG1 (% suppression was 72.8% in RMG1-HNF1β-sh1 ($P=0.041$; Figure 2A)) also caused accelerated cell proliferation as compared to control cells ($P<0.0001$; Figure 2B). PDT of RMG1-HNF1β-sh1 and RMG1-control cells by WST-8 assays were 41.9 and 65.2 h, respectively.

Effect of HNF-1β Knockdown on Cell Cycle Progression and the Expression of CDKN1A and CDKN1B

We evaluated cell cycle progression by using Nocodazole, which arrests cell cycle at G2/M phase. Non-silencing RMG2 cells were significantly retarded in the transition G1/S to G2/M phase after 12, 24 h incubation with Nocodazole, compared to HNF-1β-knockdown RMG2 cells (Figure 1C). In addition, the detection of BrdU incorporation revealed that the percentage of S-phase cell was significantly reduced in 19.9% in RMG2-control cells, compared with 29.1% in RMG2-HNF1β-sh1 and 28.9% in RMG2-HNF1β-sh2 (Figure 1D).

Since HNF-1β knockdown resulted in an increase in cell proliferation in RMG2 cells, we evaluated CDKN1A and CDKN1B expression in HNF-1β-knockdown and non-silencing RMG2 cells by Western blot. CDKN1B protein levels in both RMG2-HNF1β-sh1 and RMG2-HNF1β-sh2 were significantly repressed as compared with the RMG2-control cells (% suppressions were 61.9% and 81.8%, respectively; Figure 1E). CDKN1A protein levels were also suppressed in RMG2-HNF1β-knockdown cells compared with RMG2-control cells (% suppressions were 81.9% and 83.1%, respectively; Figure 1F).

Effect of HNF-1β Knockdown on Glucose Uptake, Glycolytic Flux, and Lactate Secretion

The rate of glucose uptake was measured using a scintillation counter and normalized to that of non-silencing control cells. Uptake of extracellular glucose was significantly decreased in HNF-1β-knockdown cells as compared to control cells (RMG2-HNF1β-sh1, 42.6 ± 6.56%, $P=0.0019$; RMG2-HNF1β-sh2, 40.2 ± 5.29% $P=0.0014$; Figure 3A).

To verify that HNF-1β promotes glycolytic activity, we further examined glycolytic flux, which was determined by measuring the rate per hour of conversion of ^{3}H-labeled glucose to H_2O through the glycolytic pathway (Figure 3B). Glycolytic flux was significantly decreased in HNF-1β-knockdown cells as compared to control cells (RMG2-HNF1β-sh1, 56.0 ± 8.78%, $P=0.0012$; RMG2-HNF1β-sh2, 49.8 ± 2.56%, $P<0.0001$; Figure 3B).

Lactate secretion into the culture media was also measured and was significantly suppressed in HNF-1β-knockdown cells (RMG2-HNF1β-sh1, 70.0 ± 6.46%, $P=0.030$ and RMG2-HNF1β-sh2, 45.2 ± 8.53%, $P=0.0047$) relative to the control cells (Figure 3C).

We also analyzed the effect of HNF-1β on glucose metabolism using another OCCC cell line, RMG1. Glucose uptake (69.0 ± 1.60%, $P=0.0008$; Figure 3D), glycolytic flux (71.5 ± 1.35%, $P=0.0003$; Figure 3E) and lactic acid production (60.0 ± 0.98%, $P<0.0001$; Figure 3F) in RMG1-HNF1β-sh1 cells were also significantly suppressed compared to control cells.

Effect of HNF-1β Overexpression on Cell Proliferation, Glucose Uptake, Glycolytic Flux, and Lactate Secretion

Expression of HNF-1β was determined by qRT-PCR and Western blot following transfection of the *HNF-1β* gene construct into Hey ovarian cancer cells. Both the mRNA and protein levels were markedly increased in Hey-HNF1β compared with the Hey-control cells (Figure 2A). Forced expression of HNF-1β in Hey cells led to a decrease in cell proliferation, as measured using the WST-8 assay ($P=0.0003$; Figure 2B). The PDT of Hey-control and Hey-HNF1β was 11.9 and 14.9 h, respectively.

Glucose uptake was significantly increased in Hey-HNF1β cells when compared with Hey-control cells (231 ± 65.2% vs. 100 ± 28.8%, $P=0.0334$; Figure 3G). Hey-HNF1β cells also exhibited enhanced glycolytic flux relative to the Hey-control cells (120 ± 7.26% vs. 100 ± 2.84%, $P=0.0099$; Figure 3H).

Lactate production over the course of 24 h was also elevated in Hey-HNF1β cells compared with that in Hey-control cells (118 ± 7.74% vs. 100 ± 8.37%, $P=0.0028$; Figure 3I).

Moreover, forced expression of HNF-1β in the immortalized human ovarian surface cell line (HOSE/E7/hTERT) showed a similar result as Hey

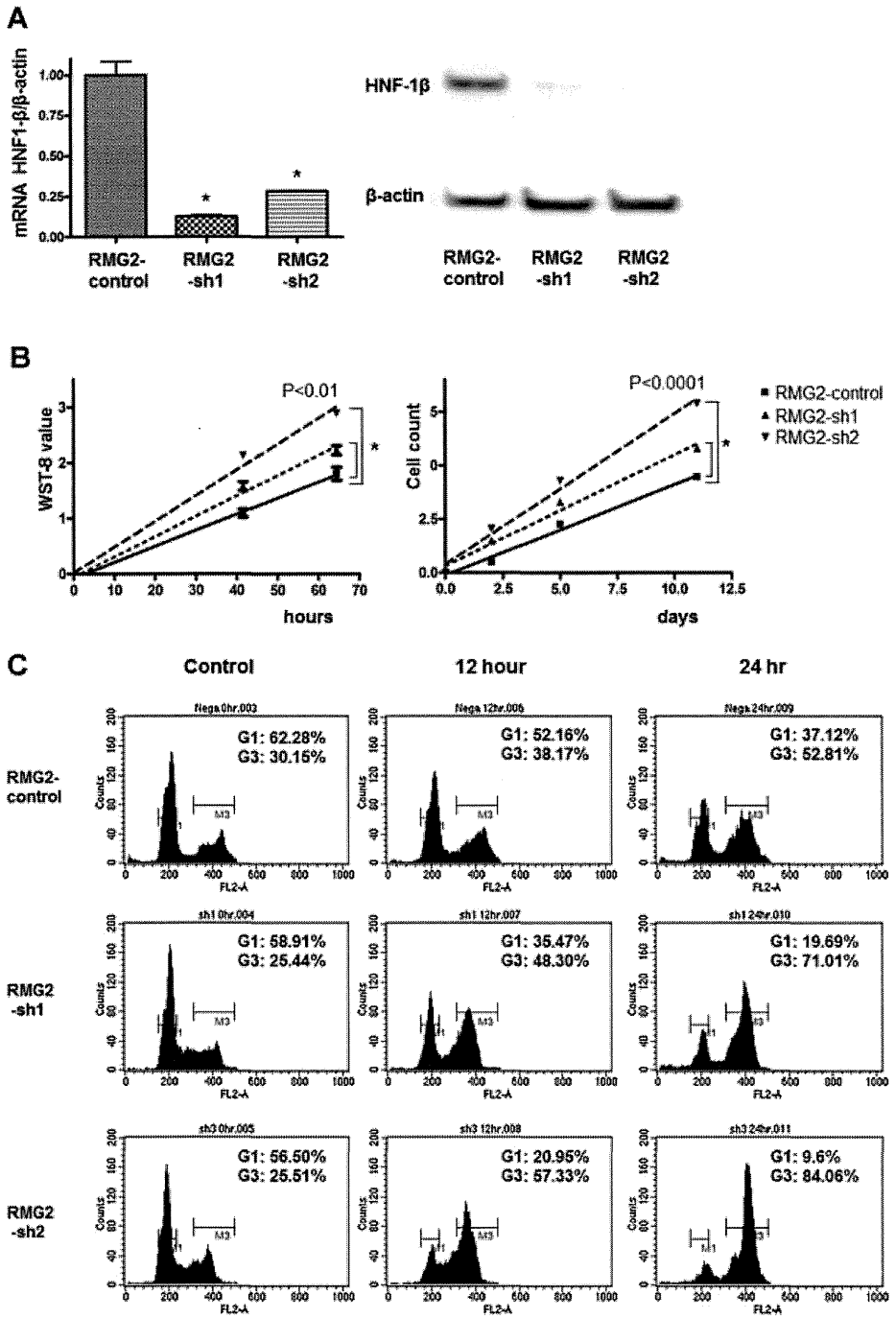

Figure 1. Short hairpin RNA mediated knockdown of HNF-1β expression enhanced cell proliferation rates with suppression of CDKN1A and CDKN1B protein expression and progressed cell cycle the G1/S to G2/M phase. (A) *HNF-1β* mRNA expression detected by quantitative RT-PCR (left panel). HNF-1β protein expression detected by Western blot analysis (right panel). (B) Cell proliferation curve produced from results of the WST-8 assay (left panel). Cell proliferation curve produced by direct cell counts (right panel). *x*-axis, incubation time; *y*-axis, relative number cells in $\log_2$ scale. In detail, relative number cells are determined as WST-8 value (number of cells) divided by WST-8 (number of cells) value at 0 h (0 d). (C) Cell cycle analysis using PI after 12, 24 h nocodazole treatment. (D) The cell cycle analysis using BrdU incorporation. (E) CDKN1B protein expression by Western blot analysis. (F) CDKN1A protein expression by Western blot analysis. The right panels of (E) and (F) showed the quantified protein expressions which were normalized with the expression in control cells. RMG2-sh1, RMG2-HNF1β-sh1; RMG2-sh2, RMG2-HNF1β-sh2; G1, G1 phase; G3, G3 phase; $^*P < 0.01$.

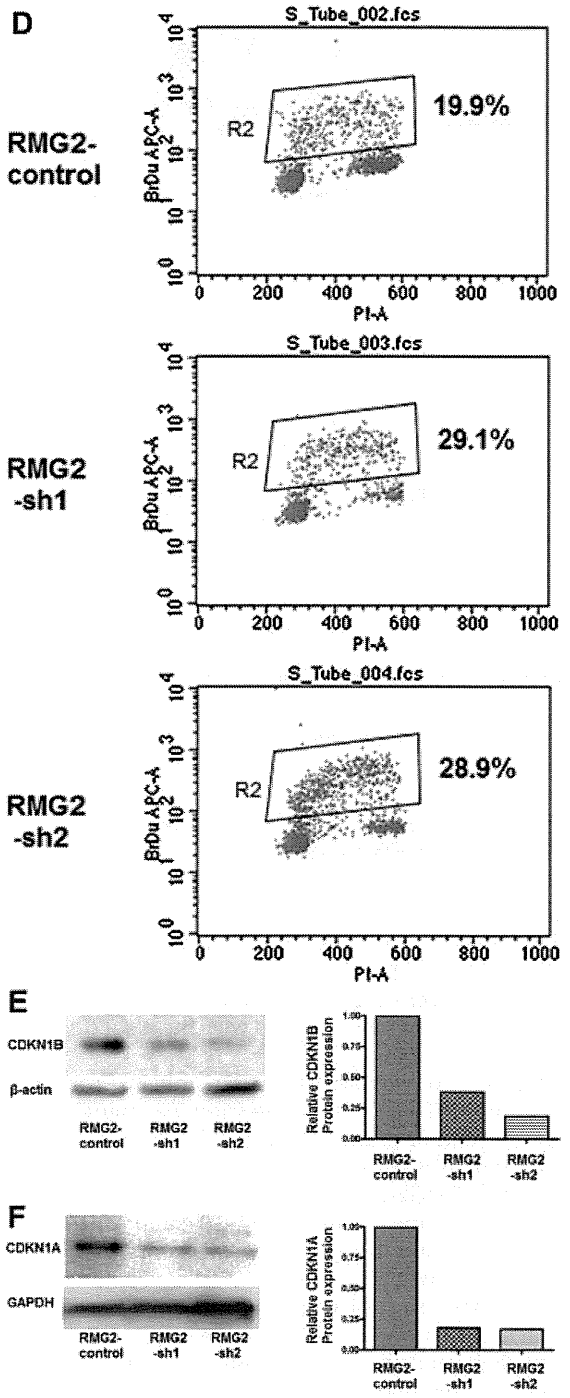

Figure 1. (*Continued*)

cell in glucose uptake, glycolytic flux and lactate production (Supplementary Figure 2).

Effect of HNF-1β Knockdown and Overexpression on GLUT1 Expression

GLUT1 mRNA expression in HNF-1β-knockdown RMG2 cells was evaluated by qRT-PCR and found to be repressed as compared to the control cells (RMG2-HNF1β-sh1, 36.3 ± 0.19%, $P = 0.0001$ and RMG2-HNF1β-sh2, 40.5 ± 0.20%, $P = 0.0001$; Figure 4A). Likewise, the expression of GLUT1 protein was also lower in the HNF-1β-knockdown cells than that observed in the non-silencing control cells (Figure 4B). In addition, the mRNA expression of *GLUT1* in RMG1-HNF1β-sh1 was also decreased as compared to control cells (84.94% ± 1.25%, $P = 0.035$; Figure 4C). GLUT1 protein expression was also suppressed in RMG1-HNF1β-sh1 (Figure 4D).

Inversely, the expression of *GLUT1* mRNA in Hey-HNF1β cells was more than 2-fold higher than that in Hey-control cells (228 ± 11.2% vs. 100 ± 0.98%, $P = 0.0073$; Figure 4E). GLUT1 protein expression was also elevated in the HNF-1β-overexpressing cells (Figure 4F).

Effect of HNF-1β Suppression on Glycolytic Enzymes and HIF-1α Expression

Messenger RNA expression levels of most of the glycolytic enzymes (Hexokinase1 (*HK1*), Hexokinase2 (*HK2*), Glucose-6-phosphate isomerase (*GPI*), Phosphofructokinase liver type (*PFK-L*), Phosphofructokinase platelet type (*PFK-P*), Aldolase A (*ALDOA*), Aldolase B (*ALDOB*), Aldolase C (*ALDOC*), Triosephosphate isomerase (*TPI*), Phosphoglycerate kinase 1 (*PGK1*), Phosphoglycerate kinase 2 (*PGK2*), Phosphoglycerate mutase 1 (*PGAM1*), Enolase 2 (*ENO2*), Enolase 3 (*ENO3*), Lactose dehydrogenase A (*LDHA*), Lactose dehydrogenase B (*LDHB*)) were significantly decreased in RMG2-HNF1β-sh1 cells as compared with the RMG2-control group (Figure 5).

Since HIF-1α is implicated in the stress-resistance in several cell lines, we examined if HNF-1β affects HIF-1α expression. Expression levels of *HIF-1α* mRNA were not significantly different between RMG2-HNF1β-sh1, RMG2-HNF1β-sh2, and RMG2-control cells (Supplementary Figure 3).

Effect of HNF-1β Suppression on OCCC Signature

OCCC signature upregulated genes (393 probe sets) were significantly enriched in the non-silencing control cell group as compared with the HNF-1β-knockdown cells (RMG2-HNF1β-sh1, RMG2-HNF1β-sh2; FDRq-value < 0.0001 and <0.0001, respectively; Figure 6A). OCCC signature downregulated genes (44 probe sets) were significantly enriched in the HNF-1β-knockdown cells when compared with the non-silencing control cells (FDRq-value = 0.0019 and 0.0051, respectively; Figure 6B). These data indicate that by suppressing HNF-1β activity, the OCCC signature profile is altered in a manner that more closely matches the non-OCCC gene signature profile.

Creation of an HNF-1β Signature From HNF-1β-knockdown Microarray Data

We analyzed the gene expression microarray data derived from the HNF-1β-knockdown cells and the

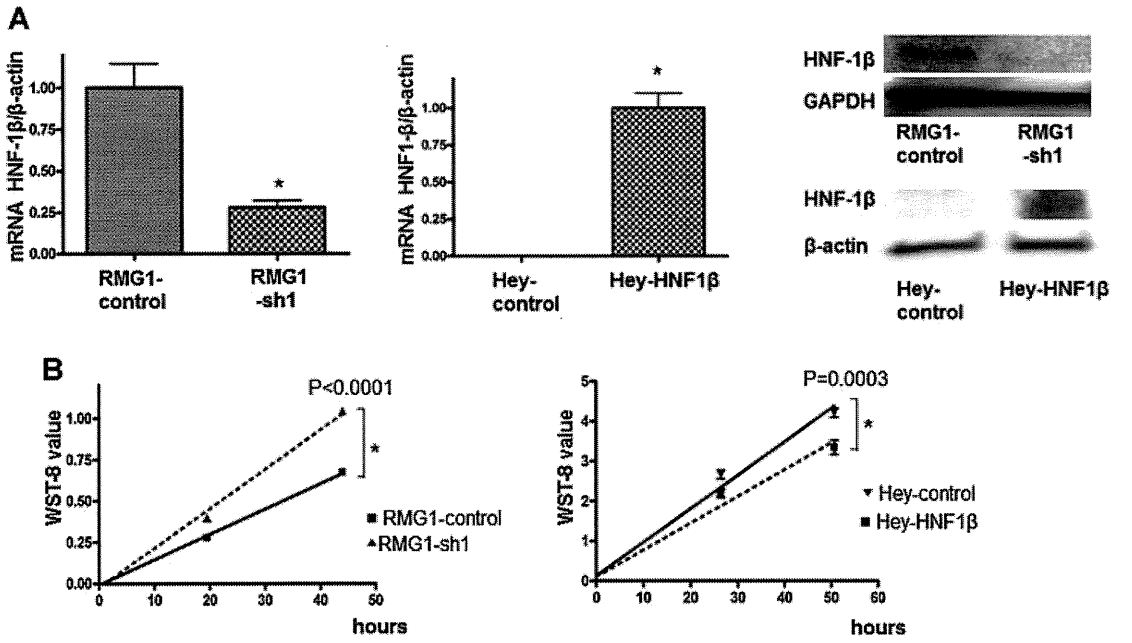

Figure 2. Knockdown of HNF-1β in RMG1 cells and forced expression of HNF-1β in Hey cells also affected the cell proliferation rate. (A) *HNF-1β* mRNA expression detected by quantitative RT-PCR (left and central panel). HNF-1β protein expression by Western blot analysis (right panel). (B) Cell proliferation curve produced from results of the WST-8 assay. RMG1-sh1, RMG1-HNF1β-sh1; $^*P < 0.05$. Experiments were done three times in triplicate.

non-silencing control cells using Bayesian binary regression 2.0, and derived an HNF-1β signature that consists of 250 probe sets (Supplementary Table 3) that are differentially expressed between these two groups (Figure 6C and D). The HNF-1β signature was able to distinguish OCCC from non-OCCC in the clinical ovarian cancer dataset GSE6008 (HNF-1β signature probability, 0.934 ± 0.0378 in OCCC vs. 0.423 ± 0.208 in non-OCCC, $P < 0.0001$) and in dataset GSE2109 (HNF-1β signature probability, 0.632 ± 0.297 in OCCC vs. 0.478 ± 0.224 in non-OCCC, $P = 0.0112$), as well as in the ovarian cancer cell line dataset KyotoOv [8] (HNF-1β signature probability, 0.610 ± 0.196 in OCCC vs.0.409 ± 0.221 in non-OCCC, $P = 0.012$; Figure 6D).

Effect of GLUT1 Knockdown on Glucose Uptake of RMG2 Cells

Knockdown of GLUT1 was performed using *GLUT1*-specific siRNAs (siRNA1, siRNA2). Over 41.8% (siRNA1) and 49.6% (siRNA2) knockdown of *GLUT1* expression was achieved as measured by qRT-PCR and 87.7% (siRNA1) and 61.7% (siRNA2) reduction in GLUT1 protein levels measured by Western blot (Supplementary Figure 1A and B). Glucose uptake following GLUT1 suppression was decreased relative to that observed in the cells receiving the negative-control siRNA (siRNA1, $73.7 \pm 7.72\%$, $P = 0.0074$; siRNA2, $70.8 \pm 6.28\%$, $P = 0.0030$; Supplementary Figure 1C).

Effect of HNF-1β Suppression on the Expression of Superoxide Dismutase 1 (*SOD1*)

In the microarray data derived from the HNF-1β-knockdown cells and the non-silencing control cells, the expression of *SOD1*, which is one of oxidative stress genes, were significantly suppressed in RMG2-HNF1β-sh1 cells ($P < 0.0001$) and RMG2-HNF1β-sh2 cells ($P = 0.0002$) as compared with the RMG2-control (Figure 6F).

Further, we validated the *SOD1* mRNA expression by using qRT-PCR. The expression was significantly decreased in RMG2-HNF1β-sh1 cells ($P = 0.0012$) and RMG2-HNF1β-sh2 cells ($P = 0.0001$) as compared with the RMG2-control (Figure 6G). Using another OCCC cell line, RMG1, HNF-1β suppression also caused decrease in mRNA expression of *SOD1* genes ($P = 0.029$; Figure 6G).

The expression of Glutathione peroxidase (*GPX*), which is also one of the oxidative stress genes, was also decreased in HNF-1β-suppressed cells (Supplementary Figure 4).

DISCUSSION

We previously identified an OCCC-specific gene expression signature that contains multiple genes with functional relevance to the biology of clear cell carcinomas, including *HIF-1α*, *IL-6*, and *HNF-1β*. In this study, we focused on the role of HNF-1β in OCCC for several reasons. First, HNF-1β is overexpressed